Made available by Hasselt University Library in https://documentserver.uhasselt.be

Interface Engineering for Highly Efficient and Stable Perovskite Solar Cells

Peer-reviewed author version

Zhao, Chenxu; Zhang , Hong; KRISHNA, Anurag; Xu, Jia & Yao, Jianxi (2023)
Interface Engineering for Highly Efficient and Stable Perovskite Solar Cells. In:
Advanced Optical Materials,.

DOI: 10.1002/adom.202301949
Handle: http://hdl.handle.net/1942/41886

Interface Engineering for Highly Efficient and Stable Perovskite Solar Cells

Chenxu Zhao[1,2], Hong Zhang[2*], Anurag Krishna,[3,4,5] Jia Xu[1], Jianxi Yao[1*]

[1]State Key Laboratory of Alternate Electrical Power System with Renewable Energy Sources, Beijing Key Laboratory of Energy Safety and Clean Utilization, North China Electric Power University, Beijing 102206, China.

[2]State Key Laboratory of Photovoltaic Science and Technology, Shanghai Frontiers Science Research Base of Intelligent Optoelectronics and Perception, Institute of Optoelectronics, Fudan University, Shanghai 200433, P. R. China.

[3]Thin Film PV Technology, Imec, imo-imomec, Thor Park 8320, 3600 Genk, Belgium

[4]EnergyVille, imo-imomec, Thor Park 8320, 3600 Genk, Belgium

[5]Hasselt University, imo-imomec, Martelarenlaan 42, 3500 Hasselt, Belgium

*Corresponding to: hzhangioe@fudan.edu.cn (H.Z.); jianxiyao@ncepu.edu.cn (J.Y.)

Abstract

The ongoing global research and development efforts on perovskite solar cells (PSCs) have led the power conversion efficiency (PCE) to a high record of 26.1%. The optimization of PSC processing methods, the development of new compositions, and the introduction of passivation strategies have been key factors behind the meteoric rise in performance. In particular, defect passivation and mitigation of ion migration via molecular engineering of the interfaces have played a critical role in enhancing the photovoltaic performance and operational stability of PSCs. This review focuses on the key interface engineering strategies enabling highly stable and efficient PSCs. We discuss the interface chemistry and the deleterious impact associated with it. The molecular design of effective modulators to mitigate the negative effects of perovskite interfaces is elaborated along with advanced characterization techniques to probe the interfaces. The progress of interface modification by multiple strategies is presented, and different modulator designs that have been proven to be effective in mitigating the negative effects of perovskite interfaces are highlighted. Moreover, the main properties of effective interface modification strategies are summarized, and general design principles are deduced for future applications. This review provides important insights into the fields of material chemistry, physical chemistry, and optoelectronics.

1. Introduction

Since the emergence of organic–inorganic lead-halide perovskite solar cells (PSCs) in 2009, PSCs have been achieving a qualitative leap in their progress and have been eliciting extensive attention from researchers worldwide, thus increasing the power conversion efficiency (PCE) to a high record of 26.1%.[1] Even though this certified PCE is close to the world-record PCE of Si-based solar cells

(26.7%), the PCE of perovskites with an ideal bandgap (Eg) of 1.34 eV under a Shockley–Queisser (S-Q) limit of ~33% can still be improved.[2] Although PSCs, especially the currently popular $FAPbI_3$-based PSCs, have great usage potential for next-generation photovoltaics,[1g, 1k, 1l, 3] they still suffer from poor operational stability and easy degradation under ambient conditions. In addition, they exert a potentially negative impact on the environment due to their toxic lead components.[3k, 4] Extensive effort has been exerted by scientists worldwide to solve these problems, and interface modification has been widely adopted to reduce the trap states and numerous crystal defects, particularly the open-circuit voltage (V_{OC}), which act as carrier recombination centers and greatly limit the photovoltaic performance of PSCs.[3b, 5] These defects, including anion vacancies and undercoordinated lead cations, which are formed mostly on the surface and grain boundaries of the perovskite layer, inevitably trigger swift ion migration, moisture penetration, and phase transition in the perovskite layer, thereby accelerating device degradation in under various standard IEC and ISOS stability test protocols.[1f, 4f, 6]

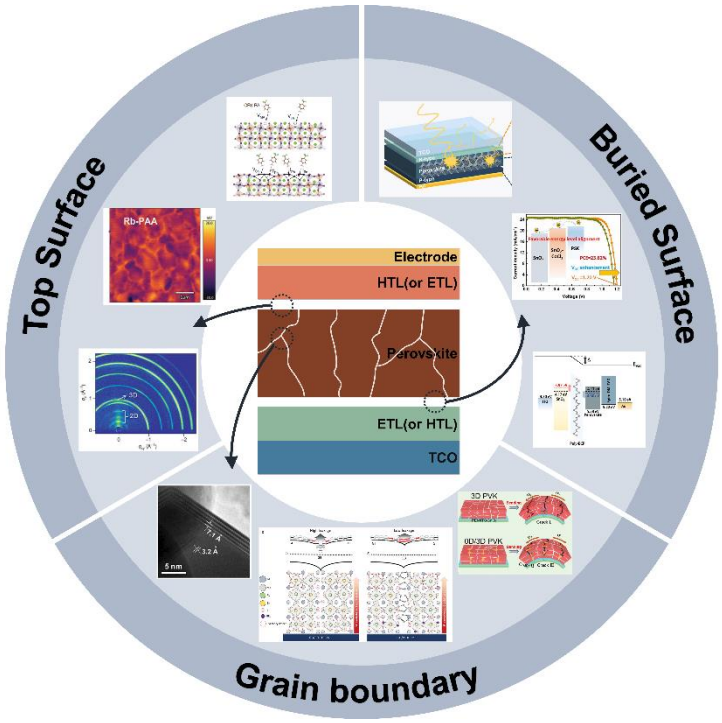

Figure 1. Perovskite interface properties. Adapted with permission.[4f] Copyright 2023, Wiley-VCH. Adapted with permission.[7] Copyright 2022, Springer Nature. Adapted with permission.[8] Copyright 2023, Elsevier. Adapted with permission.[9] Copyright 2021,American Chemical Society. Adapted with permission.[10] Copyright 2023, Wiley-VCH. Adapted with permission.[11] Copyright 2019, AAAS. Adapted with permission.[12] Copyright 2021, Wiley-VCH. Adapted with permission.[13] Copyright 2023, Wiley-VCH.

This review discusses the interface properties of PSCs and the progress of the molecular design of effective modulators for mitigating the negative effects of the perovskite interface. First, we discuss the fundamental interface properties and the characterization techniques employed to study them. Second, different modulator designs that have been proven effective in mitigating the deleterious effects of the

perovskite interface are highlighted, and possible modulation mechanisms are presented. Last, we summarize the main properties of effective interface modulators and deduce general design principles to guide their design for future applications. In the **Table 1**, we listed the device configuration and best PV parameters [the open-circuit voltage (V_{OC}), J_{SC}, FF and PCE] of the PSCs adopted different interface passivation strategies which are recently published. This review provides important insights into the fields of material chemistry, physical chemistry, and optoelectronics.

Table 1. Device configuration and best PV parameters [the open-circuit voltage (V_{OC}), J_{SC}, FF and PCE] of the PSCs adopted different interface passivation strategies.

	Device Configuration	**Interface passivation strategy**	V_{OC} [V]	J_{SC} [mA/cm^2]	**FF** [%]	**PCE** [%]	***Refs***
1	ITO/SnO_2/$(FAPbI_3)_{1-x}(MAPbBr_3)_x$/**PEAI**/Spiro-OMeTAD/Au	Surface passivation by PEAI	1.16	24.9	81.4	23.56	[5b]
2	FTO/c&m-TiO_2(Li)/$FAPbI_3$:**MACl**/PEAI/Spiro-OMeTAD/Au	Volatile MACl additives	1.130	25.92	82.02	24.02	[14]
3	ITO/PTAA/$FA_{0.6}Cs_{0.4}Pb(I_{0.65}Br_{0.35})_3$**:$Cd^+$**/$C_{60}$/$SnO_2$/ITO/PEDOT:PSS/PTAA/Cd-$FA_{0.5}MA_{0.45}Cs_{0.05}Pb_{0.5}Sn_{0.5}I_3$/$C_{60}$/BCP/Cu	Cd^+ additives	1.99	15.1	0.77	23.0	[15]
4	ITO(PEN)/SnO_2:**3AAH**/$FAPbI_3$/Spiro-OMeTAD/Ag	Pre-Buried ETL	1.187	24.45	80.47	23.36	[16]
5	ITO/SnO_2/$FA_xMA_{1-x}PbI_3$:**PAGG**/Spiro-OMeTAD/Au	**PAGG** additives	1.145	24.90	80.80	23.00	[17]
6	FTO/cTiO_2/m-TiO_2:**Li_2CO_3**/$FAPbI_3$/PEAI/Spiro-OMeTAD/Au	Li_2CO_3 modification of BIF	1.171	26.17	82.47	24.06	[18]
7	FTO/c&m-TiO_2(Li)/$(FAPbI_3)_{0.985}(MAPbBr_3)_{0.015}$:**Rb-PAA**/Spiro-OMeTAD/Au	Rb-PAA in anti-solvent	1.185	25.42	82.8	24.93	[4f]
8	ITO/SnO_2/$CsPbI_xBr_{3-x}$:**CsF**/Spiro-OMeTAD/Au	TIF modification	1.27	19.40	85.3	21.02	[19]
9	FTO/**bSnO$_2$**:**Cl**/$FAPbI_3$/Spiro-OMeTAD/Au	BIF modification	1.190	25.71	84.43	25.83	[20]
10	ITO/MeO-2PACz/CsFAMAPbBrI:***β*-FV2F**/PCBM/BCP/Ag	TIF modification	1.177	24.8	84.3	24.6	[21]
11	ITO/SnO_2/$MA_{0.25}FAPbI_3$:**[Se-MI][BF_4]**/PEAI/Spiro-OMeTAD/Au	[Se-MI][BF_4] additives	1.165	26.04	82.66	25.10	[22]
12	ITO/SnO_2/$Cs_{0.03}FA_{0.95}MA_{0.02}Pb(I_{0.975}Br_{0.025})_3$:**POF-HDDA**/Spiro-OMeTAD/Ag	POF-HDDA additives	1.201	25.72	80.13	24.76	[23]
13	FTO/cTiO_2/m-TiO_2(Li)/$FA_{0.97}MA_{0.03}PbI_{2.91}Br_{0.09}$/**TPC**/Spiro-OMeTAD/Au	Nanoscale interfacial engineering	1.17	25.2	79.1	23.4	[24]
14	ITO/SnO_2:**$CoCl_2$**/FAMAPbIBr/PEAI/Spiro-OMeTAD/Au	$CoCl_2$ doping in ETL	1.20	24.57	79.52	23.37	[9]
15	ITO/SnO_2:**RbCl**/$FA_{0.95}MA_{0.05}PbI_{0.95}Br_{0.05}$/PPEAI/Spiro-OMeTAD/Au	RbCl doping in ETL	1.184	25.05	84.5	25.14	[25]
16	ITO/NiO_x:**6FPPY**/$CsMAFAPb(IBr)_3$/PCBM/BCP/Ag	Modulating buried interface with 6FPPY	1.18	24.9	81.6	24.0	[26]

17	FTO/SnO_2/CsFAMA perovskite:**Ferrocene**/spiro-OMeTAD/Au	Ferrocene-Induced Perpetual Recovery	1.144	24.11	78.01	21.51	[27]
18	ITO/PTAA/$Cs_{0.05}FA_{0.8}MA_{0.15}PbI_{2.55}Br_{0.45}$/$C_{60}$/ALD-$SnO_2$/Au /PEDOT:PSS/ $(FASnI_3)_{0.6}(MAPbI_3)_{0.4}$:**GuaSCN** /PEAI/$C_{60}$/BCP or ALD/Cu	2D passivation layer induced by GuaSCN	1.942	15.01	80.31	23.4	[28]
19	FTO/bSnO_2/**KFSO**/$FAPbI_3$:**KFPV**/MeO-PEAI/Spiro-OMeTAD/Au	Bulk and interface engineering by KFSO/KFPV	1.17	26.12	85.22	26.04 (25.06)	[8]
20	ITO/SnO_2:**poly-BCP**/$(CsPbI_3)_{0.05}[MA_{0.03}FA_{0.97}Pb(I_{0.97}Br_{0.03})_3]_{0.95}$/OAI (PEAI)/Spiro-OMeTAD/Au	Poly-BCP doping in ETL	1.21	25.21	80.12	24.43	[10]
21	ITO/SAM/$FA_{0.8}Cs_{0.15}MA_{0.05}Pb(I_{0.82}Br_{0.18})_3$/**PEAI+MASCN**/$C_{60}$/BCP/Cu Ag/HIT/$MgF_2$	Grain regrowth and bifacial passivation	1.221	21.6	83.3	21.9 (29.8)	[29]
22	FTO/TiO_2/$Cs_{0.05}FA_{0.85}MA_{0.10}Pb(I_{0.97}Br_{0.03})_3$:**DIAI**/**DIAI**/Spiro-OMeTAD/Au	Synergistic crystallization and passivation by DIAI	1.176	25.06	81.89	24.13	[30]
23	FTO/**TiO_xN_y**/meso-TiO_2/PMMA:PCBM/$Cs_{0.05}FA_{0.9}MA_{0.05}PbI_{2.74}Br_{0.26}$/PMMA/P3HT:CuPc/Au	Nitrogen-doped titanium oxide electron	1.200	22.89	85.1	23.38	[31]
24	ITO/NiO_x/CsMAFAPb(IBr)$_3$:**PPP**/PCBM+C60/BCP/ Cr/Au	PPP additives in anti-solvent	1.131	23.24	84.1	22.11	[32]
25	FTO/TiO_2/SnO_2/$Cs_{0.05}MA_{0.05}FA_{0.9}PbI_3$/**BAI**/Spiro-OMeTAD/Au	2D/3D Heterojunction	1.159	26.01	83.9	25.32	[33]
26	ITO/Me-4PACz/**Al_2O_3 nanoplate**/1.55-eV Perovskite/LiF/C_{60} /BCP/Cu	Porous insulator contact at BIF	1.208	25.08	84.37	25.56	[34]
27	ITO/NiO_X/VNPB/WBG/C_{60}/SnO_2/Au/PEDOT:PSS/NBG:**CF_3-PA**/C_{60} /BCP/Cu	CF_3-PA additives	2.03	16.5	79.9	26.7	[7]
28	FTO/bSnO_2/KCl/$FAPbI_3$:**PACl**/MeO-PEAI/Spiro-OMeTAD/Au	Volatile PACl additives	1.179	25.8	84.6	25.73 (26.08)	[35]
29	ITO/NiO/SAM/$FA_{0.8}Cs_{0.2}Pb(I_{0.62}Br_{0.38})_3$/$C_{60}$/ALD-$SnO_2$/Au /PEDOT:PSS/ $FA_{0.7}MA_{0.3}Pb_{0.5}Sn_{0.5}I_3$/**FL-WBG**/PEAI/$C_{60}$/BCP or ALD/Cu	3D/3D bilayer heterojunction	2.112	16.5	81.9	28.5	[36]
30	FTO/SnO_2/$FAPbI_3$:**$(PbI_2)_2RbCl$**/PEAI/Spiro-OMeTAD/Au	$(PbI_2)_2RbCl$ stabilizer	1.182	26.3	82.7	25.6 (26.1)	[37]
31	Ag/ITO/nc-Si:H(p)/a-SiH(i)/c-Si/a-SiH(i/n)/nc-Si:H(n+/p+)/ITO/Me-4PACz /$Cs_{0.18}FA_{0.82}Pb(I,Br)_3$:**FBPAc**/$C_{60}$/$SnO_X$/IZO/Ag	FBPAc additives	1.91	20.47	79.8	31.25	[38]

2. Perovskite interface properties and characterizations

2.1 Interface chemistry in perovskite films

The typical device configurations for PSCs include normal (n-i-p) and inverted (p-i-n) structures. Regardless of the specific configuration, PSCs have the two interfaces between perovskite and charge transport layers (CTLs): buried interface (BIF) and top surface/interface. Meanwhile, polycrystalline perovskite films derived from a solution process exhibit tremendous structural disorder in their grain boundaries, and they can be regarded as the third kind of interface. The performance, including the short-circuit current density (J_{SC}), fill factor (FF), and open-circuit voltage (V_{OC}), of PSCs is strongly related to the recombination of defects in the bulk or at the interfaces of the perovskite layer.[5b, 39] However, defects have been theoretically predicted to be shallow.[40] Suppression of shallow defects in polycrystalline perovskite films, especially at interfaces, is a crucial and effective way of further enhancing the overall performance and operational stability of PSCs, and it is currently in demand because it can meet the requirements of commercialization from laboratories to industries.[5b] The interfaces are where defects are most easily formed, and the passivation of interface defects is the most important task in all types of solar cells.[1g, 1i, 8]

In an ideal PSC crystal structure, each atom is fixed at its position, but the actual crystal structure is influenced by the crystal growth process and post-treatment, resulting in defects. Four main types of defects at interfaces have been identified as critical sources of nonradiative recombination: (1) intrinsic point defects, including anti-site, vacancy, and interstitial defects, which can introduce a transition level in the forbidden band, and when the transition level is close to the valence or conduction band, shallow-level defects occur; (2) 2D extended defects, including grain boundaries and surface defects;[41] and (3) 3D defects, such as lead clusters. Notably, although the strong nonradiative processes at the defective surface of films or crystals are detrimental to solar energy conversion, they can result in interesting applications of perovskite materials, such as narrow-band photodetectors. Most point defects with low formation energies have been reported to result in shallow-level traps and thus have a negligible contribution to nonradiative recombination, which possibly explains the large diffusion lengths and high defect tolerance of organic–inorganic PSC materials. However, due to the ionic nature of perovskite materials and high ion migration speed, charged point defects can migrate to interfaces under an electric field and influence the photovoltaic performance of PSCs and long-term stability. Therefore, it is imperative to passivate both deep and shallow defects for achieving highly efficient and stable PSCs.

2.2 Characterization techniques for studying the interfaces in PSCs

The microstructure of the polycrystal perovskite layer is essential in achieving high operational stability, good photovoltaic performance, and successful upscaling of high-quality perovskite thin films for commercialization. Therefore, a reliable and accurate characterization of the thin-film microstructure is paramount, and summary of characterization measurements applied to probing defect passivation in perovskite solar cell research is shown in **Fig. 2** and **Table S1**.[42] Accurate knowledge of the thickness, surface roughness, work function, complex refractive index or complex dielectric constant, and optical bandgap (E_g) of perovskite films is essential for the design of optoelectronic devices (**Fig. 2b**).[43] An

ideal homogeneous perovskite thin film has an optimum thickness that can balance the contradiction between absorption rate and carrier transmission distance.[44] Surface roughness can strongly affect light scattering.[45] The complex refractive index or dielectric function tensor, which provides access to fundamental physical parameters, is related to various sample properties, including morphology, crystal quality, chemical composition, and electrical conductivity.[46] X-ray diffraction (XRD)-based characterization techniques, including conventional laboratory-based XRD and synchrotron-based grazing-incidence wide-angle X-ray scattering (GIWAXS) (**Fig. 2c**), are widely used to provide information on a material's crystallographic structure, phases, preferred crystal orientations, chemical composition, and other physical properties related to the crystallinity of the material.[47] Performing XRD experiments, such as GIWAXS, in a synchrotron facility can provide additional microstructural information, such as depth-dependent and quantitative film texture information, and in-situ experiments can allow for a real-time assessment of the evolution of the microstructure during processing.[42, 47] Scanning electron microscopy (SEM) and atomic force microscopy (AFM) is real-space imaging techniques that are commonly utilized to characterize thin-film morphology, such as surface coverage, grain size, and surface roughness.[48] Additional microstructural information can also be obtained through SEM characterizations, such as phase separation and distribution by detecting characteristic X-rays or backscattered electrons. Advanced AFM-based techniques, such as Kelvin probe force microscopy and conductive AFM, can further correlate the local microstructure of perovskite thin films to local electronic and photovoltaic properties.[49] Transmission electron microscopy (TEM)-based techniques, such as selected-area electron diffraction, high-resolution TEM, and scanning TEM, can probe the atomic-scale microstructure through electron diffraction and atomic-resolution real-space imaging, thus providing useful microstructural information, such as lattice spacings and structural imperfections (e.g., dislocation, twinning, and stacking faults from a highly localized area on the scale of nanometers).[48, 50] The application of TEM-based techniques, however, requires extra care because hybrid perovskite materials can easily be damaged by the electron beam due to their fragile nature; such damage can generate artifacts in the results.[50b, 50c, 51] Moreover, deep mechanistic comprehension of PSCs requires new, suitable in situ imaging techniques, and the development of operando characterization methods is necessary for further progress. Typically, capacitance measurements, such as drive-level capacitance profiling,[52] space-charge-limited current,[53] deep-level transient spectroscopy,[39] and spectrometric characterization methods, such as photoluminescence (PL) quantum yield, calculated quasi-Fermi level splitting,[5a, 6c] and steady-state PL emission[54] and in situ techniques, are new emerging characterization tools that may be used to achieve an in-depth understanding of PSC materials.[55]

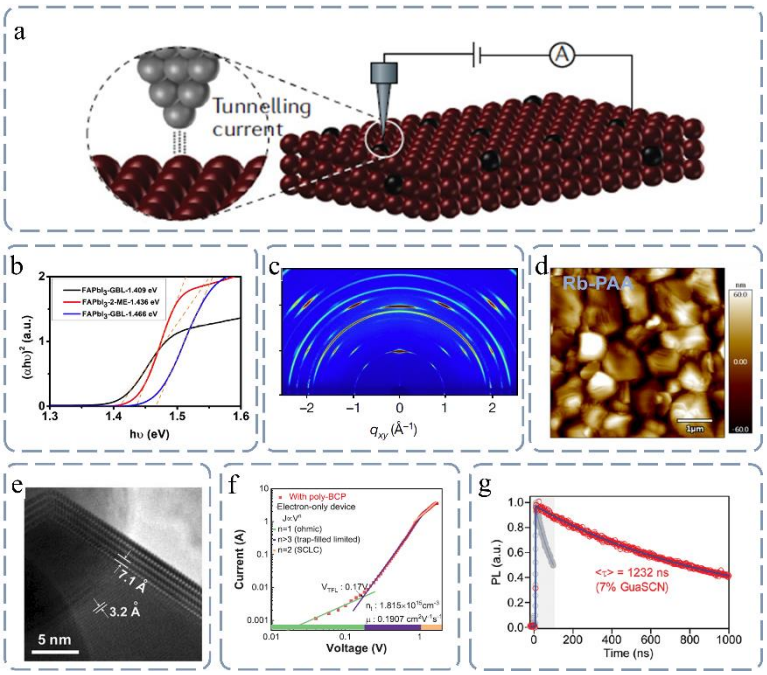

Figure 2. Summary of characterization measurements applied to probing defect passivation in perovskite solar cells. Copyright. Part (**a**) was adapted with permission.[56] Copyright 2020, Springer Nature. Part (**b**) was adapted with permission.[57] Copyright 2022, Wiley-VCH. Part (**c**) was adapted with permission.[35] Copyright 2023, Springer Nature. Part (**d**) was adapted with permission.[4f] Copyright 2023, Wiley-VCH. Part (**e**) and (**g**) was adapted with permission.[11] Copyright 2019, AAAS. Part (**f**) was adapted with permission.[10] Copyright 2022, Wiley-VCH.

3. Strategies to mitigate the negative effects of the perovskite interface

3.1 Manipulation of perovskite crystallization

3.1.1 Buried interface modification

Recently, increased attention has been paid to the buried interface **(**BIF) between the underlying CTL and perovskite film, especially after the planar structure has taken center stage in PSCs. BIF plays a critical role in manipulating crystallization, extracting photogenerated carriers, and regulating band energy matching. Poor-quality BIF with massive defects leads to inferior crystallinity of the perovskite bulk, as shown in Fig.3. Ionic salts, such as KCl,[3k] KF,[58] and NH_4F,[59] and functional organic compounds, such as zwitterions,[60] self-assembled monolayers,[61] 2-methylbenzimidazole,[62] benzylamine hydrochloride,[63] and phosphate[64], have been proposed as chemicals to passivate the surface of SnO_2. Amine salts as organic additives have also been utilized to modify BIF, especially pre- and post-treatment in SnO_2 CTL in the n-i-p structure. BIF modification is bottom–up strategy to obtain high-quality underlying CTL, and it can facilitate the crystalline growth of the perovskite layer.[34, 65] Consequently, the release of residual stresses inside perovskite bulks promotes the transition of the perovskite from thermodynamic instability to thermodynamic stability with microcompressive stresses during annealing and cooling periods. Additionally, the defects at BIF and the bulk defects of perovskite

can be inhibited considerably. Amine salts are also likely to form a 2D perovskite layer at the bottom interface, templating the crystal growth of the perovskite layer.[66]

Organic molecules can act as bridges to connect the underlying CTL and perovskite layer, thus enhancing the energy level matching and conductivity. The multifluorine organic molecule 6FPPY can bridge the NiO_x/perovskite interface through moieties with F atoms, thus producing a NiO_x film with high hole transport efficiency, releasing the residual strain of the perovskite film, passivating the NiO_x/perovskite interface defects, and suppressing the detrimental reaction between NiO_x and perovskite.[67] Bathocuproine-based nonconjugated polyelectrolyte acts as a "dual-side passivation layer" between the SnO_2 underlying CTL and the perovskite absorber, and it suppresses the bulk and interfacial nonradiative recombination by passivating oxygen-vacancy defects from the SnO_2 side and simultaneously scavenges ionic defects from the other (perovskite) side; it has a high PCE of 24.4% and a high open-circuit voltage of 1.21 V with a reduced voltage loss (perovskite bandgap of 1.56 eV).[68]

Recently, p-type self-assembled monolayers (SAMs) have been widely used to modify the surface properties of the underlying CTL and improve the performance of inverted PSCs.[69] SAMs with different dipole moments have been adopted for the following reasons: (i) to serve as a "binder" to improve the adhesion between the underlying CTL and the perovskite layer and facilitate charge transfer by passivating the inorganic surface trap states,[70] (ii) to modify the work function of the underlying CTL through molecular ordering induced by the permanent dipole moments,[71] and (iii) to change the perovskite crystallinity and morphology through chemical interactions of different terminated functional groups.[72] Benefiting from the crystallization regulation and both fast extraction and efficient passivation at the hole-selective interface, SAMs, Me-4PACz, could also slow light-induced halide segregation of a tandem-relevant perovskite composition with 1.68-eV bandgap, lead to high single-junction device V_{OC} values of >1.23 V, and a certified power conversion efficiency of 29.15% for monolithic perovskite/silicon tandem.[73]

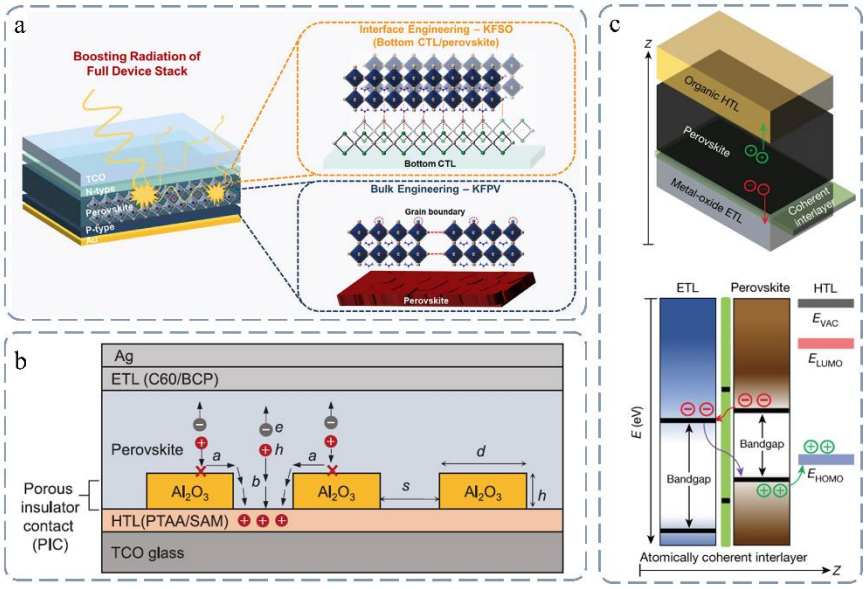

Figure 3 Buried interface modification. (a) schematic illustration of the research direction and strategies for reaching the radiative limit of PCE. Adapted with permission.[8] Copyright 2023, Elsevier. **(b)** Photovoltaic performance improvement in inverted structure by introducing a thick (about 100 nanometers) porous insulator contact (PIC) layer with random nanoscale openings. Adapted with permission.[34] Copyright 2023, AAAS. **(c)** Up, layered stack of the ETL, perovskite, and HTL, with an interlayer between the perovskite absorber and the ETL. Down, energy diagrams of the ETL, perovskite, and HTL. Adapted with permission.[1g] Copyright 2021, Springer Nature.

The buried surfaces of perovskite films are more prone to deterioration and defect formation than the bulk and upper surfaces of perovskite films due to continuous solvent and temperature erosion processes. Alkali metal salts have been reported to passivate the interfacial defects at the SnO_2/perovskite BIF, cation vacancy, and grain boundary of perovskite films. KCl, KI, KOH, and KFSO have been introduced to passivate the interfacial defects at BIF and the bulk defect of perovskite, thus improving the photovoltaic performance and alleviating the hysteresis of PSCs (**Fig. 3a**).[4c, 8, 74] A buried-interface strategy using rubidium (Rb)-based perovskitoids has been proposed, and the introduction of Rb halide has been found to result in the formation of a deuterogenic Rb-based perovskitoid "scaffold," which effectively enhances the crystallization of the perovskite film and passivates the defects on the buried surface.[25] With this Rb-based perovskitoid strategy, the PCE of devices increases from 23.26% to 25.14%. The strategy provides a simple and effective way to improve the performance of PSCs. A previous study also introduced cobalt chloride hexahydrate ($CoCl_2 \cdot 6H_2O$) into a SnO_2 film, which showed favorable energy level alignment and good charge extraction; correspondingly, an enhanced V_{OC} of up to 1.20 V was achieved along with an efficiency of 23.82%, which is the record open-circuit voltage at the optical band gap of 1.54 eV in planar-structure PSCs.[75] Moreover, a coherent interlayer is formed between a perovskite thin film and a Cl-bonded SnO_2 (Cl-bSO) electrode coated with a Cl-containing $FAPbI_3$ perovskite precursor (Cl-cPP). A crystalline $FASnCl_x$ phase forms as an atomically

coherent solution interlayer at BIF (**Fig. 3c**). This interlayer reduces the interfacial charge recombination loss and contact resistance, enabling the fabrication of a PSC with a PCE of 25.8%.[1g]

3.1.2 Additives

Additive-based strategies are widely applied to perovskite precursor solutions to obtain efficient and highly stable PSCs, and they play an indispensable role at every stage of breakthrough and improvement in the photovoltaic performance and operational stability of PSCs, as shown in **Fig. 4**. Additives can modulate the morphology of perovskite films, stabilize the phase of formamidinium (FA)- and cesium (Cs)-based perovskites, adjust energy level alignment in PSCs, suppress nonradiative recombination in perovskites, eliminate hysteresis, and enhance the operational stability of PSCs.[76] Various kinds of additives, including inorganic salts, molecules, polymers, and even nanoparticles, are utilized. The diversity of available additives results from the good coordination of the lead cation and iodide anion in halide perovskites, which is also the foundation for solution processing of PSCs.[76-77]

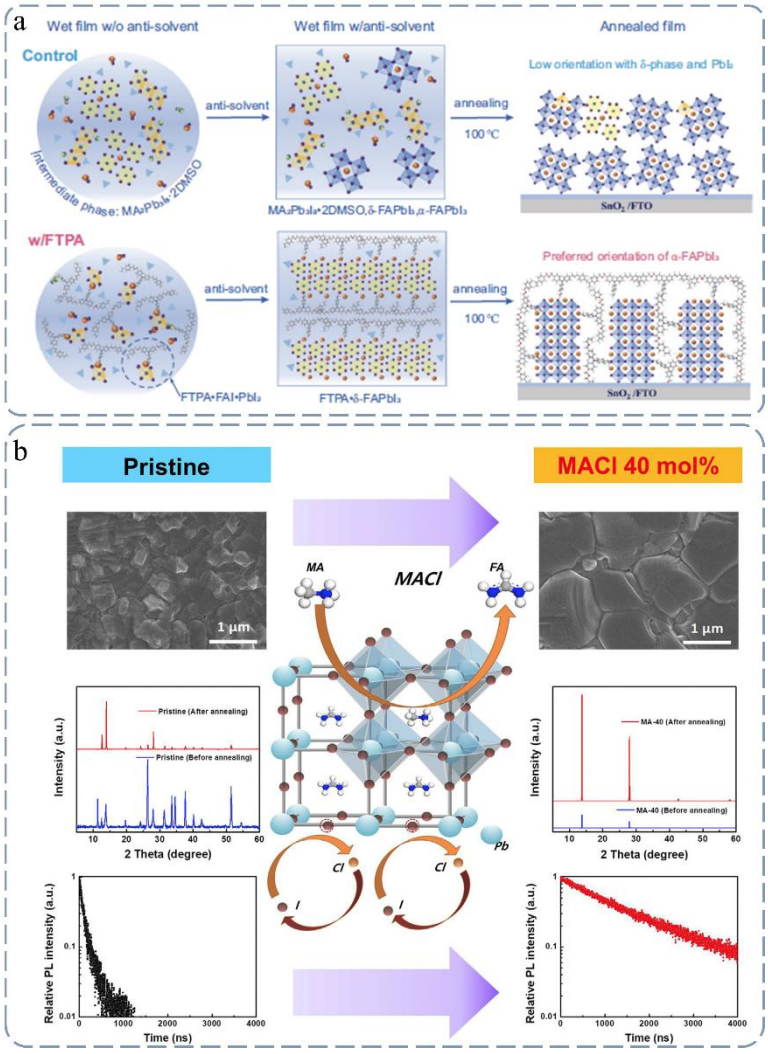

Figure 4 Additives engineering. (a) possible phase evolution of the nucleation and crystallization of FA-based mixed anion perovskites ($FA_{0.95}MA_{0.05}Pb(I_{0.95}Br_{0.05})_3$) during the film-forming process with (w) or without (w/o)

FTPA. Perovskite film with FTPA restrained the formation of the intermediate phases and formed a hydrogen-bonding polymer network in the perovskite films which induced stable and preferred orientation of α-$FAPbI_3$. Adapted with permission.[77d] Copyright 2023, Springer Nature. **(b),** The MACl addition could induce the intermediate phase with pure a-phase without annealing, effectively stabilizing the structure, only through cationic site substitution. Adapted with permission.[77c] Copyright 2019, Elsevier.

The coordination between the lead cation and iodine anion from perovskites with ions from salt additives via the ionic bond can be easily understood.[78] Alkali metal cations have been widely explored and interstitial doped, such as Li^+, Na^+, K^+, or Rb^+, to suppress the migration of halide ions, alleviate current-voltage hysteresis, and improve operational stability.[4f, 37, 74b, 79] While benefiting from their smaller radiuses, the incorporation of K^+ and Rb^+ ions won't form K or Rb-based photoactive perovskite phase without sacrificing spectral absorption range. In particular, K^+ remains the presence of unreacted KX (X=I, Br, or Cl) in the prepared perovskite films.[79a] On the other hand, similar to K, Rb is unable to form a stable perovskite alloy with FA^+, but forms rubidium-rich non-perovskite phases, which can mitigate the ions migration and passivates the defects at the grain boundary and interfaces.[4f, 37] The doping of divalent (Ca^{2+}, Cd^{2+}) or trivalent (Nd^{3+}) could also appreciably prevent halide migration in the perovskite lattice with a minimal dose addition, and the higher valence state would provide a better capability to obstruct halide migration and lead to advantageous device performance by the perovskite solar cell with a substantially lower dopant concentration.[15, 80] For molecular additives, the coordination of perovskite with additives is generally through a coordinate bond because the lead cation can be treated as Lewis acid, which can coordinate with the Lewis base molecule, and the iodine anion can be treated as Lewis base, which can coordinate with the Lewis acid molecule.[76] Available polymer additives for PSCs generally possess Lewis acid or base groups, such as carbonyl and amino, and coordinate with perovskites via the coordinate bond.[81] For nanoparticle additives with a molecular or covalent crystal structure, the interaction may proceed via the coordinate bond.[82] For nanoparticle additives with an ionic crystal structure, the interaction may be through the ionic bond.[5b, 77c, 83] The introduction and existence form of additives for PSCs differ.[84] Some additives are introduced into the precursor before film preparation, and some are introduced into the film during postprocessing. Some additives are removed after device fabrication, and some still remain in the devices.[3k, 83b, 85] Some of the remaining additives grow in the crystal, and some grow at the boundaries and on the surfaces or interfaces.[86]

Additives also play a critical role in perovskite-based tandem solar cells, especially in the all perovskite tandem solar cells. The emergency of all-perovskite tandem solar cells gives a promise of higher PCE than single-junction PSCs while maintaining a low fabrication cost, enabling the high potential of commercialization in the future.[7, 15, 28, 36] Based on the highly demand of high efficiency mixed Pb–Sn narrow-bandgap subcells, a thick mixed Pb–Sn perovskite layer is needed to achieve even higher photocurrent density, accompanying with comparable high V_{OC} and fill factor. That means the

challenge of the short carrier diffusion length within Pb–Sn perovskites should be properly alleviated, which is mainly induced by more complex and severe defect doping within narrow-bandgap subcells compared to their Pb-based counterparts.[15] 4-trifluoromethyl-phenylammonium (CF_3-PA) was developed by Renxing Lin and his coworkers as additives in the mixed Pb–Sn perovskite precursor solution, which was proved only partially adsorbed on the surface defective sites at perovskite crystallization temperatures by molecular dynamics simulations. The stronger perovskite surface-passivator (CF_3-PA) interaction facilitated the significant increasing of the carrier diffusion length within Pb–Sn perovskites to over 5 μm, which enabled the PCEs enhancement of Pb–Sn perovskite solar cells to over 22% and all-perovskite tandem solar cells to a certified efficiency of 26.4%.[7] What's more, another key in the perovskite-based tandem devices is the halide segregation in the wide bandgap perovskite solar cell, which would lead to high nonradiative recombination rates at their interfaces and severe V_{OC} loss.[87] Xin Yu Chin et. al introduced 2,3,4,5,6-pentafluorobenzylphosphonic acid (FBPAc) into FABr:FAI solution and coated on a silicon bottom cell, which could regulate the crystallization process of wide bandgap perovskite and alleviate recombination losses occurring at the perovskite top surface interfacing the electron-selective contact, resulting in a certified power conversion efficiency of 31.25%.[38]

3.1.3 Antisolvent

The nonpolar washing process during the spin coating of perovskite films (called the antisolvent process) was first reported by Xiao et al. and Jeon et al. in 2014 independently, and it pushed perovskite development to a new era, as shown in **Fig. 5a**.[88] Conventional spin-coating results in a shiny gray film composed of non-uniform large crystals as a result of slow crystallization. In the antisolvent process (**Fig. 5a** bottom), a second solvent (e.g. chlorobenzene) introduced on top of the wet film during the spin-coating process induces fast crystallization of uniformly sized perovskite grains.[88b] To date, the most advanced PSCs with PCEs that are close to the world record value of 26% are still mainly based on the antisolvent process. Doping in an antisolvent is an easy and important means to control perovskite crystallization and passivate interior defects. The doping of passivators in an antisolvent allows the passivators to enter deeply into the perovskite bulk and passivate the internal grain boundary, even for organic molecules with large domain sizes and long chains.

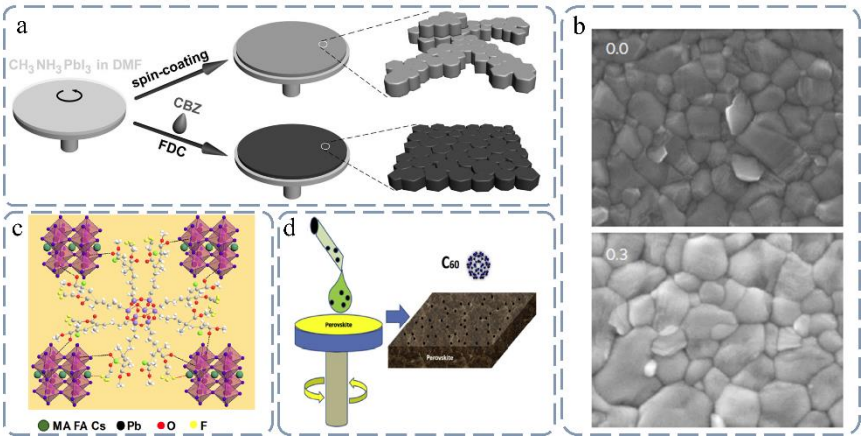

Figure 5 Antisolvent engineering. (a) Schematic illustration of the conventional spin-coating process (top) and the antisolvent process (bottom) for fabricating perovskite films (top). Adapted with permission.[88b] Copyright 2014, Wiley-VCH. **(b)** Top SEM of perovskite films deposited by antisolvent doped with different concentrations (mg/ml) of PMMA. Adapted with permission.[89] Copyright 2016, Springer Nature. **(c)** Schematic diagram of the interaction between the 3D star-shaped polyhedral (PPP polymer) and perovskite, including chelation between C═O and Pb and hydrogen bonding between ─CF_3 and FA^+ and MA^+. Adapted with permission.[90] Copyright 2021, AAAS. **(d)** Toluene doped with a small amount of fullerene (C60) as an antisolvent in the fabrication process. Adapted with permission.[91] Copyright 2018, Elsevier.

Various macromolecular organic compounds or polymers have been explored as anti-solvents to impart perovskite solar cells with high-quality, outstanding performance.[4f, 89-90, 92] Poly(methyl methacrylate), abbreviated as PMMA, has been used as an additive in a mixed solvent of chlorobenzene and toluene, and polymer-templated nucleation and growth have been proven to be effective methods for crystal engineering.[89] Trace amounts of PMMA doping in the antisolvent (0.6 mg/mL) can uniformly trigger heterogeneous nucleation over the perovskite precursor film, thus improving the grain size and allowing the perovskite to grow in a preferred direction (**Fig. 5d** and **5e**). A high doping concentration of PMMA (>0.6 mg/mL) diminishes photovoltaic performance because of the intrinsic high insulation. Conjugated polymers (PF-0, PF-1, N2200, and F-N2200) have also been introduced as additives in chlorobenzene, and they can improve charge transport because of their superior ability to optimize the surface morphology, reduce interface defects, and tune p/n-type properties.[92b] Qi Cao et al. proposed a novel modulator, namely, a 3D star-shaped polyhedral (**Fig. 5b**), and doped it in an antisolvent to regulate the crystallization inside the perovskite bulk.[90, 92c] This star-shaped polyhedral exhibits outstanding hydrophobic, antiadhesion properties[92a] and passivates defects at the grain boundaries and interfacial surfaces through its polymer branches with multiple chemical anchor sites, which enables an optimal PCE of 22.1% with an extremely high FF value of 86.2% and outstanding operational stability.

The fullerene family, which has been confirmed to have passivated defects and enhanced electrical properties at the hole transport layer (HTL)/perovskite interface, has also been introduced into the

antisolvent system. Ji et al. used C60 fullerene (**Fig. 5c**) and toluene to fabricate an $MAPbI_3$ film.[91] Their results showed that C60 enhances the crystallinity of perovskite, effectively passivates surface defects, and restricts ion diffusion. These improvements result in a PCE of 19.8% for C60 modified devices. Wu et al. utilized a fullerene derivative [6,6]-phenyl-C61-butyric acid methyl ester (PCBM)–toluene solution and dripped it on a perovskite film during spin coating to create a graded heterojunction. During solvent removal (DMSO) by an antisolvent (toluene), some PCBM (which was present in the antisolvent solution) was trapped inside the perovskite film due to the interaction between PCBM and lead halide complexes, which led to a graded heterojunction. This type of heterojunction was proven to be highly efficient for electron injection, interface trap density reduction, hysteresis elimination, and high stability. A certified efficiency of 18.21% was achieved from the fabricated PSCs (FA based) with an aperture area of 1.022 cm^2. In addition, α-bis-PCBM has been utilized in a chlorobenzene antisolvent treatment method to improve perovskite film quality. The addition of α-bis-PCBM induces the uniform heterogeneous nucleation and directional growth of perovskite grains. Electron-accepting α-bis-PCBM enhances the electron transfer ability and provides good stability to devices. These improvements lead to excellent PCEs (above 20%) of α-bis-PCBM-based PSCs. Moreover, small molecules and organic dyes have been explored via the antisolvent dripping method to improve perovskite film quality and achieve efficient charge collection and enhanced stability.[93]

3.1.4 Secondary crystallization growth

The disordered arrangement of molecules at grain boundaries would act as the starting point for ion migration and fast degradation, the ion migration activation energy increases along with the increase in the crystal grain size.[94] The perovskite single-crystal devices without grain boundaries showed negligible current hysteresis and no ion migration signal.[95] Therefore, increasing the grain size to decrease the grain boundary areas is one of the effective strategies for better operational stability of PSCs.[95] Secondary crystallization growth (SCG), induced by Oswald aging process,[29, 96] was regarded as an important means to achieve larger grain sizes and better crystallinity, where grain size and crystallinity are increased, the internal grain boundaries are reconstructed, and surface chemistry is optimized to improve PSC performance. The first step in SCG is the fabrication of fresh PSCs by several means, among which solution processing is the most used method. The second step is the post-treatment-induced regrowth of as-prepared perovskite films (**Fig. 6a**).

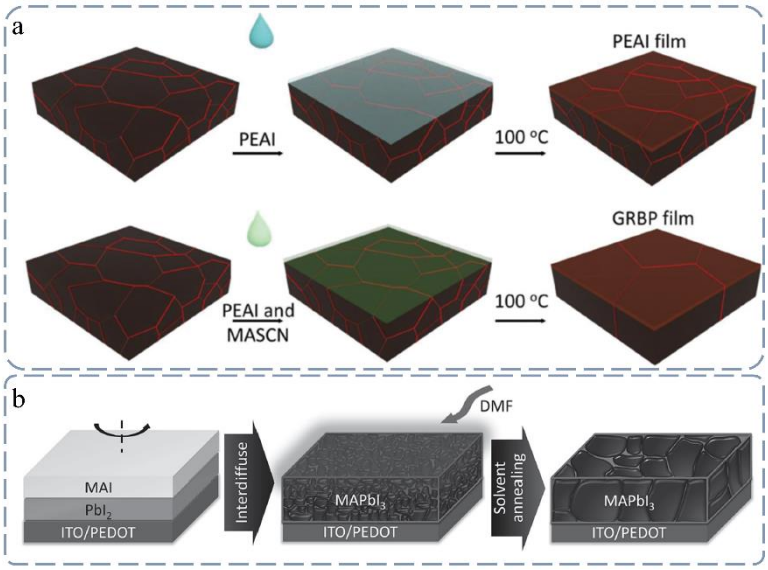

Figure 6 Secondary crystallization growth. (a) schematic illustration of post-treatment-induced regrowth of as-prepared perovskite films. Adapted with permission.[29] Copyright 2023, Wiley-VCH. **(b)** the illustration of the SCG induced by solution vapor assist. Adapted with permission.[97] Copyright 2014, Wiley-VCH.

Amine salt solution is commonly used in the solution-processed SCG method (SCG-S), and the adoption of MACl in SCG-S was first reported by Xie et al.[83a] The MACl solution is deposited on the surface of pre-prepared, yellow, δ-phase $FAPbI_3$ perovskite films, and the MACl molecule vertically diffuses into the perovskite bulk to trigger the transformation from δ phase to α phase upon annealing. Through the SCG-S process induced by MACl, FA-based perovskite films with high crystallinity are obtained, and they demonstrate good performance with a PCE of 20.65% and high stability. A simple methylammonium bromide (MABr) treatment with a optimized MABr concentration can also lead to the SCG-S process in a $MAPbI_3$-based perovskite system, which is then converted to high-quality $MAPbI_{3-x}Br_x$ thin films.[96] When MABr is substituted by MAI with an optimal concentration, perovskite crystallinity improves slightly, and the degree of grain growth is much more limited compared with that in MABr post-treatment. The SCG-S process of perovskite is not simply implemented from excess organic amine groups; the halogen anion exchange (I-Br) reaction with the Ostwald ripening process is also important and the most possible mechanism of the SCG-S process. Rui Zhu et al. applied a guanidinium bromide solution to a group on the surface of as-prepared perovskite films to react with excess PbX_2 crystals (X is a mixture of I and Br) surrounding the perovskite grains; the application facilitated the recrystallization and grain regrowth of perovskite films.[98] Chloride-based molecules (FACl and MACl) have also been explored in an Sn-based perovskite system in the SCG-S process; they result in a reduction in nonradiative recombination and improved photovoltaic performance.[99] Pseudohalogenated ammonium salt can also trigger the SCG-S process. MASCN induces the regrowth of perovskite grains and simultaneously facilitates the penetration of PEAI into the HTL/perovskite bottom interface. Consequently, the bulk and interface nonradiative recombination

losses are reduced, and the open-circuit voltage in solar cells is considerably increased. PCEs of 21.9% and 19.9% are obtained for 1.65-eV-bandgap opaque and semitransparent perovskite solar cells, respectively.[29]

Aside from the SCG-S method, SCG induced by solution vapor assist (SCG-V) has also been explored by many researchers. Xiao et al. were the first to adopt the SCG-V method and DMF vapor to provide a polar environment, where the grain size is significantly enlarged to more than 1 μm, with material electronic property improvement and performance enhancement of photovoltaic devices to 15.6% (**Fig. 6b**).[97] Liu et al. further revealed the SCG-V mechanism by constructing a mixed-polar-solvent vapor system (DMSO, DMF, and γ-butyrolactone).[100] The mixed polar vapor can condense on the perovskite films' surface during the annealing process to dissolve the perovskite crystal and form a phase between solid and liquid phases. During the period of dynamic balance between recrystallization by solvent molecule evaporation and redissolution of minor grains, the perovskite films grow gradually and become increasingly dense and compact with enhanced crystallinity and few grain boundaries; they exhibit a PCE of 13%. Xiao et al. found that the utilization of MABr/DMSO mixed vapor in the SCG-V process can form an $MA_2Pb_3I_8(DMSO)_2$ intermediate phase located at the perovskite grain boundaries, which enhances grain boundary migration kinetics and photovoltaic performance to 17.64% from 15.13% (pristine PSCs).[101] Regular antisolvents and their mixtures have also been explored in the SCG-V process. For example, Li et al. used chlorobenzene (PhCl) to improve the quality of film perovskite films.[102] Yu et al. optimized the ratio of mixed solvent vapor (DMF and PhCl) to realize ultrasmooth $MAPbI_xCl_{3-x}$ films with a PCE of 16.4%.[103] The antisolvent vapor of *o*-dichlorobenzene or PhCl was introduced by Xianggao Li et al., who found that antisolvent molecules from vapor can inhibit solvent evaporation during annealing, which can advance the dissolution of perovskite minor crystallites and is beneficial to SCG along the surfaces of large grains.[104]

3.2 Molecular-engineered perovskite interface via post-treatment

Given that the bandgap voltage deficiency of PSCs is still larger than that of traditional single crystal solar cells, such as GaAs cells with a bandgap voltage offset value (W_{OC}) of 0.3V, alleviating the W_{OC} of PSCs and obtaining a high V_{OC} that is as close to the S-Q limit as possible will lead to a considerable improvement in photovoltaic performance. The S-Q limit of V_{OC} is mainly contributed by radiative recombination loss, which means that nonradiative recombination should be as low as possible or completely eliminated. Previous studies have proven that the voltage losses of PSCs are primarily caused by nonradiative recombination via the defects on the top surface or top interfaces (TIF) between the perovskite and top CTL (**Fig. 7**). The ions accumulation at TIF induced by migration would normally be attributed to the inferior operational stability and low photovoltaic performance of PSCs. Post-treatment strategies, such as interface passivation, have been widely applied to minimize the nonradiative recombination losses at the top interfaces and mitigate the ions migration and accumulation, thus improve the open-circuit voltage of devices and the long-term stability under different conditions. Post-treatment strategies are predominantly employed by introducing

macromolecular polymers,[105] organic molecules,[6c, 106] inorganic materials,[107] 2D perovskite,[108] 3D perovskite[109], and others.

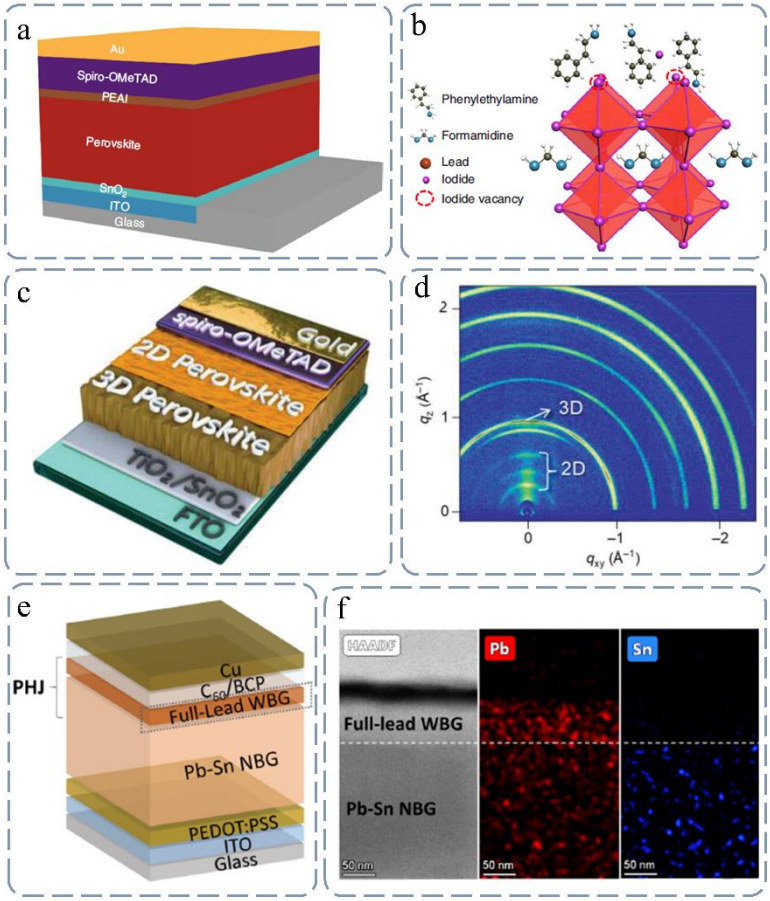

Figure 7 Molecular-engineered perovskite interface via post-treatment. (a) The device structure of the perovskite solar cells with the organic molecule (PEAI) for post-treatment. (**b**) Possible passivation mechanism of the PEAI layer for the perovskite film. Part **(a)** and **(b)** was adapted with permission.[5b] Copyright 2019, Springer Nature. **(c)** Material structure and photoelectrical properties of the 2D/3D perovskite heterojunctions, where the 2D perovskite is fabricated by post-treatment on the 3D perovskite surface. **(d)** GIWAXS patterns of the 2D/3D perovskite with BAI post-treatment. Part **(c)** and **(d)** was adapted with permission.[110] Copyright 2023, Wiley-VCH. **(e)** The schematic structure of Pb-Sn PSCs with 3D/3D bilayer perovskite heterojunction (PHJ). **(f)** Cross-sectional HR-STEM image and corresponding energy-dispersive X-ray (EDX) mapping of Pb-Sn PSCs with PHJ. Part **(e)** and **(f)** was adapted with permission.[109a] Copyright 2023, Springer Nature.

Specifically, the 2D passivation layer is an effective strategy to form a graded interface and passivate interface defects via post-treatment. Amine salts with different chain lengths are coated on the top of a 3D perovskite film, and a thermally driven uniform distribution of self-passivated 2D/3D perovskites in the bulk covered by graded mixed-dimensional, wide-bandgap 2D perovskite layers is achieved (**Fig. 7c**). This multifunctional approach not only suppresses the nonradiative recombination loss in the bulk and at the interface of the perovskite but also inherits the salient stability of 2D perovskites, thereby

dramatically increasing the efficiency and external environmental stability of PSCs.[111] 2D perovskites can be classified as Ruddlesden–Popper (RP)[112] and Dion–Jacobson (DJ) phases.[113] DJ-phase 2D perovskites show great potential for fabricating 2D/3D bilayer PSCs due to their superior carrier transport, strengthened layered structure, and increased stability in comparison with RP-phase analogues.[113a, 114] Thus far, many organic spacer cations have been applied to construct DJ 2D/3D bilayer PSCs, such as octyldiammonium (ODA^{2+}),[115] 2,2-(ethylenedioxy)bis(ethylammonium) ($EDBE^{2+}$),[116] 1,4-butanediamine (BDA),[117] and 1,8-octanediammonium (ODA^{2+})[118]. The use of DJ 2D perovskites as capping layers on the upper surface of 3D perovskite films can facilely passivate surface defects, optimize interfacial energy level alignment, increase film quality and stability, and suppress the ion penetration from the perovskite layer into the HTL or substitution to the ion immune hole transport layer material, thereby boosting the efficiency and environmental stability of PSCs.

Despite the inherent merits of the 2D/3D heterojunction that alleviate interfacial recombination losses, the increase in the series resistance of PSCs hampers free charge transport and thus limits the device fill factors due to the asymmetric conductivity and potentially nonuniform distributions.[109] The 3D perovskite passivation layer, as a new type of heterojunction that can be used as a substitute for the commonly used 2D interlayer, can fundamentally mitigate the trade-off between surface passivation and passivation layer conductivity. 3D perovskites are much more conductive than 2D interlayers. Doping a 3D/3D bilayer in narrow-bandgap (Pb-Sn mixed) PSCs results in a favorable type-II band alignment at the top interface, as shown in **Fig. 6e** and **6f**, which can facilitate charge transport and thus increase PCE to a high level of 23.8%, with a high FF of over 82%.[109a] A world-record PCE of 28% for all-perovskite tandem solar cells has been obtained.[119]

4. Summary and outlook

Metal halide perovskites have emerged as wonder materials for optoelectronic devices. In particular, the progress in photovoltaic (PV) devices based on these hybrid perovskite materials has been unprecedented. In light of low manufacturing costs and appealing device performance, the levelized cost of electricity (LCOE) of perovskite PVs has the potential to reach impressively low levels to drive the global energy transition economically. However, despite the promises, the commercialization of PSCs is impeded by low device stability. Grain boundary and interface defects are one of the main driving factors for instability and performance loss. In this review, we have summarized the interface chemistry in PSCs and the strategies for the molecular design of effective modulators to mitigate the deleterious effects of the perovskite interface. The characterization techniques for understanding the interfaces were discussed, and the development of operando characterization methods for obtaining deep mechanistic comprehension of PSCs was presented. We have discussed the passivation of the buried interface, top interface, and grain boundaries. We have presented different passivation methodologies and highlighted the effectiveness of these strategies for improving the PCE and stability. Since the PCE of single-junction cells has reached over 26%, the focus is shifting toward upscaling and

fabrication of large-area modules. However, the majority of the interface engineering strategies have been shown for small area cells (<1 cm^2). Therefore, there is a need to validate these passivation strategies on large-area modules. Moreover, for commercialization cost and reproducibility are key factors, therefore passivation materials that are developed should be cost-effective, must be easily processable by industrial-compatible deposition techniques, and have good reproducibility. Therefore, more efforts should be devoted to developing low-cost and robust interface passivation materials which can meet the requirements of commercialization.

Reference:

[1] a)Y. Zhao, F. Ma, Z. Qu, S. Yu, T. Shen, H.-X. Deng, X. Chu, X. Peng, Y. Yuan, X. Zhang, J. You, *Science* **2022**, 377, 531; b)L. G. Wang, H. P. Zhou, J. N. Hu, B. L. Huang, M. Z. Sun, B. W. Dong, G. H. J. Zheng, Y. Huang, Y. H. Chen, L. Li, Z. Q. Xu, N. X. Li, Z. Liu, Q. Chen, L. D. Sun, C. H. Yan, *Science* **2019**, 363, 265; c)S. Sidhik, Y. Wang, M. De Siena, R. Asadpour, A. J. Torma, T. Terlier, K. Ho, W. Li, A. B. Puthirath, X. Shuai, A. Agrawal, B. Traore, M. Jones, R. Giridharagopal, P. M. Ajayan, J. Strzalka, D. S. Ginger, C. Katan, M. A. Alam, J. Even, M. G. Kanatzidis, A. D. Mohite, *Science* **2022**, 377, 1425; d)J. W. Lee, S. Tan, S. I. Seok, Y. Yang, N. G. Park, *Science* **2022**, 375, eabj1186; e)R. Lin, K. Xiao, Z. Qin, Q. Han, C. Zhang, M. Wei, M. I. Saidaminov, Y. Gao, J. Xu, M. Xiao, *Nature Energy* **2019**, 4, 864; f)H. Zhang, F. T. Eickemeyer, Z. Zhou, M. Mladenovic, F. Jahanbakhshi, L. Merten, A. Hinderhofer, M. A. Hope, O. Ouellette, A. Mishra, P. Ahlawat, D. Ren, T. S. Su, A. Krishna, Z. Wang, Z. Dong, J. Guo, S. M. Zakeeruddin, F. Schreiber, A. Hagfeldt, L. Emsley, U. Rothlisberger, J. V. Milic, M. Gratzel, *Nat Commun* **2021**, 12, 3383; g)H. Min, D. Y. Lee, J. Kim, G. Kim, K. S. Lee, J. Kim, M. J. Paik, Y. K. Kim, K. S. Kim, M. G. Kim, T. J. Shin, S. Il Seok, *Nature* **2021**, 598, 444; h)Q. Jiang, J. Tong, Y. Xian, R. A. Kerner, S. P. Dunfield, C. Xiao, R. A. Scheidt, D. Kuciauskas, X. Wang, M. P. Hautzinger, R. Tirawat, M. C. Beard, D. P. Fenning, J. J. Berry, B. W. Larson, Y. Yan, K. Zhu, *Nature* **2022**, 611, 278; i)S. Macpherson, T. A. S. Doherty, A. J. Winchester, S. Kosar, D. N. Johnstone, Y. H. Chiang, K. Galkowski, M. Anaya, K. Frohna, A. N. Iqbal, S. Nagane, B. Roose, Z. Andaji-Garmaroudi, K. W. P. Orr, J. E. Parker, P. A. Midgley, K. M. Dani, S. D. Stranks, *Nature* **2022**, 607, 294; j)D. H. Kim, J. B. Whitaker, Z. Li, M. F. A. M. van Hest, K. Zhu, *Joule* **2018**, 2, 1437; k)H. Zhang, C. Zhao, J. Yao, W. C. H. Choy, *Angew Chem Int Ed Engl* **2023**, 62, e202219307; l)A. Kojima, K. Teshima, Y. Shirai, T. Miyasaka, *J Am Chem Soc* **2009**, 131, 6050.

[2] S. Ruhle, *Sol Energy* **2016**, 130, 139.

[3] a)J. W. Yoo, J. Jang, U. Kim, Y. Lee, S. G. Ji, E. Noh, S. T. Hong, M. Choi, S. Il Seok, *Joule* **2021**, 5, 2420; b)H. Zhang, K. Darabi, N. Y. Nia, A. Krishna, P. Ahlawat, B. Guo, M. H. S. Almalki, T. S. Su, D. Ren, V. Bolnykh, L. A. Castriotta, M. Zendehdel, L. Pan, S. S. Alonso, R. Li, S. M. Zakeeruddin, A. Hagfeldt, U. Rothlisberger, A. Di Carlo, A. Amassian, M. Gratzel, *Nat Commun* **2022**, 13, 89; c)H.-S. Yun, H. W. Kwon, M. J. Paik, S. Hong, J. Kim, E. Noh, J. Park, Y. Lee, S. Il Seok, *Nature Energy* **2022**, 7, 828; d)T. Bu, L. K. Ono, J. Li, J. Su, G. Tong, W. Zhang, Y. Liu, J. Zhang, J. Chang, S. Kazaoui, F. Huang, Y.-B. Cheng, Y. Qi, *Nature Energy* **2022**, 7, 528; e)D. Liu, D. Luo, A. N. Iqbal, K. W. P. Orr, T. A. S. Doherty, Z. H. Lu, S. D. Stranks, W. Zhang, *Nat Mater* **2021**, 20, 1337; f)Y. Vaynzof, *Nature Energy* **2021**, 6, 578; g)C. Liu, Y. Yang, K. Rakstys, A. Mahata, M. Franckevicius, E. Mosconi, R. Skackauskaite, B. Ding, K. G. Brooks, O. J. Usiobo, J. N. Audinot, H. Kanda, S. Driukas, G. Kavaliauskaite, V. Gulbinas, M. Dessimoz, V. Getautis, F. De Angelis, Y. Ding, S. Dai, P. J. Dyson, M. K. Nazeeruddin, *Nat Commun* **2021**, 12, 6394; h)Z. L. Guo, A. K. Jena, G. M. Kim, T. Miyasaka, *Energ Environ Sci* **2022**, 15, 3171; i)G. D. Niu, X. D. Guo, L. D. Wang, *J Mater Chem A* **2015**, 3, 8970; j)S. Tan, T. Huang, I. Yavuz, R. Wang, T. W. Yoon, M. Xu, Q. Xing, K. Park, D. K. Lee, C. H. Chen, R. Zheng, T. Yoon, Y. Zhao, H. C. Wang,

D. Meng, J. Xue, Y. J. Song, X. Pan, N. G. Park, J. W. Lee, Y. Yang, *Nature* **2022**, 605, 268; k)J. J. Yoo, G. Seo, M. R. Chua, T. G. Park, Y. Lu, F. Rotermund, Y. K. Kim, C. S. Moon, N. J. Jeon, J. P. Correa-Baena, V. Bulovic, S. S. Shin, M. G. Bawendi, J. Seo, *Nature* **2021**, 590, 587; l)NREL, 2022.

[4] a)J. M. Azpiroz, E. Mosconi, J. Bisquert, F. De Angelis, *Energ Environ Sci* **2015**, 8, 2118; b)J. H. Li, X. L. Liu, J. Xu, J. Chen, C. X. Zhao, M. S. Maneo, B. Zhang, J. X. Yao, *Sol Rrl* **2019**, 3, 1900218; c)P. Zhu, S. Gu, X. Luo, Y. Gao, S. Li, J. Zhu, H. Tan, *Advanced Energy Materials* **2020**, 10, 1903083; d)Q. Lou, Y. Han, C. Liu, K. Zheng, J. Zhang, X. Chen, Q. Du, C. Chen, Z. Ge, *Advanced Energy Materials* **2021**, 11, 2101416; e)S. Wang, Y. Jiang, Emilio J. Juarez-Perez, Luis K. Ono, Y. Qi, *Nature Energy* **2016**, 2, 16195; f)C. Zhao, H. Zhang, M. Almalki, J. Xu, A. Krishna, F. T. Eickemeyer, J. Gao, Y. M. Wu, S. M. Zakeeruddin, J. Chu, J. Yao, M. Gratzel, *Adv Mater* **2023**, 35, e2211619.

[5] a)P. Caprioglio, M. Stolterfoht, C. M. Wolff, T. Unold, B. Rech, S. Albrecht, D. Neher, *Advanced Energy Materials* **2019**, 9, 1901631; b)Q. Jiang, Y. Zhao, X. Zhang, X. Yang, Y. Chen, Z. Chu, Q. Ye, X. Li, Z. Yin, J. You, *Nature Photonics* **2019**, 13, 460; c)J. Peng, J. I. Khan, W. Z. Liu, E. Ugur, T. Duong, Y. L. Wu, H. P. Shen, K. Wang, H. Dang, E. Aydin, X. B. Yang, Y. M. Wan, K. J. Weber, K. R. Catchpole, F. Laquai, S. De Wolf, T. P. White, *Advanced Energy Materials* **2018**, 8, 1801208; d)C. M. Wolff, P. Caprioglio, M. Stolterfoht, D. Neher, *Adv Mater* **2019**, 31, e1902762.

[6] a)F. Wang, S. Bai, W. Tress, A. Hagfeldt, F. Gao, *Npj Flex Electron* **2018**, 2, 22; b)T. C. Sum, N. Mathews, *Energ Environ Sci* **2014**, 7, 2518; c)T. S. Su, F. T. Eickemeyer, M. A. Hope, F. Jahanbakhshi, M. Mladenovic, J. Li, Z. Zhou, A. Mishra, J. H. Yum, D. Ren, A. Krishna, O. Ouellette, T. C. Wei, H. Zhou, H. H. Huang, M. D. Mensi, K. Sivula, S. M. Zakeeruddin, J. V. Milic, A. Hagfeldt, U. Rothlisberger, L. Emsley, H. Zhang, M. Gratzel, *J Am Chem Soc* **2020**, 142, 19980; d)W. C. Yang, H. L. Long, X. Sha, J. S. Sun, Y. X. Zhao, C. Y. Guo, X. C. Peng, C. H. Shou, X. Yang, J. Sheng, Z. H. Yang, B. J. Yan, J. C. Ye, *Advanced Functional Materials* **2022**, 32, 2110698; e)B. Li, Y. Zhang, L. Fu, T. Yu, S. Zhou, L. Zhang, L. Yin, *Nat Commun* **2018**, 9, 1076; f)D. Bi, X. Li, J. V. Milic, D. J. Kubicki, N. Pellet, J. Luo, T. LaGrange, P. Mettraux, L. Emsley, S. M. Zakeeruddin, M. Gratzel, *Nat Commun* **2018**, 9, 4482; g)I. L. Braly, D. W. deQuilettes, L. M. Pazos-Outón, S. Burke, M. E. Ziffer, D. S. Ginger, H. W. Hillhouse, *Nature Photonics* **2018**, 12, 355; h)N. K. Noel, A. Abate, S. D. Stranks, E. S. Parrott, V. M. Burlakov, A. Goriely, H. J. Snaith, *ACS Nano* **2014**, 8, 9815.

[7] R. Lin, J. Xu, M. Wei, Y. Wang, Z. Qin, Z. Liu, J. Wu, K. Xiao, B. Chen, S. M. Park, G. Chen, H. R. Atapattu, K. R. Graham, J. Xu, J. Zhu, L. Li, C. Zhang, E. H. Sargent, H. Tan, *Nature* **2022**, 603, 73.

[8] M. J. Jeong, C. S. Moon, S. Lee, J. M. Im, M. Y. Woo, J. H. Lee, H. Cho, S. W. Jeon, J. H. Noh, *Joule* **2023**, 7, 112.

[9] P. Wang, B. Chen, R. Li, S. Wang, N. Ren, Y. Li, S. Mazumdar, B. Shi, Y. Zhao, X. Zhang, *Acs Energy Lett* **2021**, 6, 2121.

[10] J.-H. Kim, Y. R. Kim, J. Kim, C.-M. Oh, I.-W. Hwang, J. Kim, S. Zeiske, T. Ki, S. Kwon, H. Kim, A. Armin, H. Suh, K. Lee, *Advanced Materials* **2022**, 34, 2205268.

[11] J. Tong, Z. Song, D. H. Kim, X. Chen, C. Chen, A. F. Palmstrom, P. F. Ndione, M. O. Reese, S. P. Dunfield, O. G. Reid, J. Liu, F. Zhang, S. P. Harvey, Z. Li, S. T. Christensen, G. Teeter, D. Zhao, M. M. Al-Jassim, M. F. A. M. van Hest, M. C. Beard, S. E. Shaheen, J. J. Berry, Y. Yan, K. Zhu, *Science* **2019**, 364, 475.

[12] H. Kim, J. W. Lee, G. R. Han, S. K. Kim, J. H. Oh, *Advanced Functional Materials* **2021**, 31, 2008801.

[13] H. Liu, H. Han, J. Xu, X. Pan, K. Zhao, S. F. Liu, J. Yao, *Adv Mater* **2023**, 35, e2300302.

[14] M. Kim, G.-H. Kim, T. K. Lee, I. W. Choi, H. W. Choi, Y. Jo, Y. J. Yoon, J. W. Kim, J. Lee, D. Huh, H. Lee, S. K. Kwak, J. Y. Kim, D. S. Kim, *Joule* **2019**, 3, 2179.

[15] Z. Yang, Z. Yu, H. Wei, X. Xiao, Z. Ni, B. Chen, Y. Deng, S. N. Habisreutinger, X. Chen, K. Wang, J. Zhao, P. N. Rudd, J. J. Berry, M. C. Beard, J. Huang, *Nature Communications* **2019**, 10, 4498.

[16] Y. Meng, C. Liu, R. Cao, J. Zhang, L. Xie, M. Yang, L. Xie, Y. Wang, X. Yin, C. Liu, Z. Ge, *Advanced Functional Materials* **2023**, 33, 2214788.
[17] Y. Zhao, P. Zhu, M. Wang, S. Huang, Z. Zhao, S. Tan, T.-H. Han, J.-W. Lee, T. Huang, R. Wang, J. Xue, D. Meng, Y. Huang, J. Marian, J. Zhu, Y. Yang, *Advanced Materials* **2020**, 32, 1907769.
[18] M. Kim, I.-w. Choi, S. J. Choi, J. W. Song, S.-I. Mo, J.-H. An, Y. Jo, S. Ahn, S. K. Ahn, G.-H. Kim, *Joule* **2021**, 5, 659.
[19] X. Chu, Q. Ye, Z. Wang, C. Zhang, F. Ma, Z. Qu, Y. Zhao, Z. Yin, H.-X. Deng, X. Zhang, J. You, *Nature Energy* **2023**, 8, 372.
[20] H. Min, D. Y. Lee, J. Kim, G. Kim, K. S. Lee, J. Kim, M. J. Paik, Y. K. Kim, K. S. Kim, M. G. Kim, T. J. Shin, S. Il Seok, *Nature* **2021**, 598, 444.
[21] G. Li, Z. Su, L. Canil, D. Hughes, M. H. Aldamasy, J. Dagar, S. Trofimov, L. Wang, W. Zuo, J. J. Jerónimo-Rendon, M. M. Byranvand, C. Wang, R. Zhu, Z. Zhang, F. Yang, G. Nasti, B. Naydenov, W. C. Tsoi, Z. Li, X. Gao, Z. Wang, Y. Jia, E. Unger, M. Saliba, M. Li, A. Abate, *Science* **2023**, 379, 399.
[22] Y. Shen, G. Xu, J. Li, X. Lin, F. Yang, H. Yang, W. Chen, Y. Wu, X. Wu, Q. Cheng, J. Zhu, Y. Li, Y. Li, *Angewandte Chemie International Edition* **2023**, 62, e202300690.
[23] J. Zhang, Z. Li, F. Guo, H. Jiang, W. Yan, C. Peng, R. Liu, L. Wang, H. Gao, S. Pang, Z. Zhou, *Angewandte Chemie International Edition* **2023**, 62, e202305221.
[24] A. Krishna, H. Zhang, Z. Zhou, T. Gallet, M. Dankl, O. Ouellette, F. T. Eickemeyer, F. Fu, S. Sanchez, M. Mensi, S. M. Zakeeruddin, U. Rothlisberger, G. N. Manjunatha Reddy, A. Redinger, M. Grätzel, A. Hagfeldt, *Energ Environ Sci* **2021**, 14, 5552.
[25] J. Chen, H. Dong, J. Li, X. Zhu, J. Xu, F. Pan, R. Xu, J. Xi, B. Jiao, X. Hou, K. Wei Ng, S.-P. Wang, Z. Wu, *Acs Energy Lett* **2022**, 7, 3685.
[26] H. Wang, W. Zhang, B. Wang, Z. Yan, C. Chen, Y. Hua, T. Wu, L. Wang, H. Xu, M. Cheng, *Nano Energy* **2023**, 111, 108363.
[27] Q. Chang, F. Wang, W. Xu, A. Wang, Y. Liu, J. Wang, Y. Yun, S. Gao, K. Xiao, L. Zhang, L. Wang, J. Wang, W. Huang, T. Qin, *Angewandte Chemie International Edition* **2021**, 60, 25567.
[28] J. Tong, Z. Song, D. H. Kim, X. Chen, C. Chen, A. F. Palmstrom, P. F. Ndione, M. O. Reese, S. P. Dunfield, O. G. Reid, J. Liu, F. Zhang, S. P. Harvey, Z. Li, S. T. Christensen, G. Teeter, D. Zhao, M. M. Al-Jassim, M. F. A. M. van Hest, M. C. Beard, S. E. Shaheen, J. J. Berry, Y. Yan, K. Zhu, *Science* **2019**, 364, 475.
[29] Z. Liu, C. Zhu, H. Luo, W. Kong, X. Luo, J. Wu, C. Ding, Y. Chen, Y. Wang, J. Wen, Y. Gao, H. Tan, *Advanced Energy Materials* **2023**, 13, 2203230.
[30] X. Du, J. Zhang, H. Su, X. Guo, Y. Hu, D. Liu, N. Yuan, J. Ding, L. Gao, S. Liu, *Advanced Materials* **2022**, 34, 2204098.
[31] J. Peng, F. Kremer, D. Walter, Y. Wu, Y. Ji, J. Xiang, W. Liu, T. Duong, H. Shen, T. Lu, F. Brink, D. Zhong, L. Li, O. Lee Cheong Lem, Y. Liu, K. J. Weber, T. P. White, K. R. Catchpole, *Nature* **2022**, 601, 573.
[32] Q. Cao, Y. Li, H. Zhang, J. Yang, J. Han, T. Xu, S. Wang, Z. Wang, B. Gao, J. Zhao, X. Li, X. Ma, S. M. Zakeeruddin, W. E. I. Sha, X. Li, M. Grätzel, *Science Advances* **2021**, 7, eabg0633.
[33] W. Yang, B. Ding, Z. Lin, J. Sun, Y. Meng, Y. Ding, J. Sheng, Z. Yang, J. Ye, P. J. Dyson, M. K. Nazeeruddin, *Advanced Materials* **2023**, 35, 2302071.
[34] W. Peng, K. Mao, F. Cai, H. Meng, Z. Zhu, T. Li, S. Yuan, Z. Xu, X. Feng, J. Xu, M. D. McGehee, J. Xu, *Science* **2023**, 379, 683.
[35] J. Park, J. Kim, H.-S. Yun, M. J. Paik, E. Noh, H. J. Mun, M. G. Kim, T. J. Shin, S. I. Seok, *Nature* **2023**, 616, 724.
[36] R. Lin, Y. Wang, Q. Lu, B. Tang, J. Li, H. Gao, Y. Gao, H. Li, C. Ding, J. Wen, P. Wu, C. Liu, S. Zhao, K.

Xiao, Z. Liu, C. Ma, Y. Deng, L. Li, F. Fan, H. Tan, *Nature* **2023**, 620, 994.
[37] Y. Zhao, F. Ma, Z. Qu, S. Yu, T. Shen, H.-X. Deng, X. Chu, X. Peng, Y. Yuan, X. Zhang, J. You, *Science* **2022**, 377, 531.
[38] X. Y. Chin, D. Turkay, J. A. Steele, S. Tabean, S. Eswara, M. Mensi, P. Fiala, C. M. Wolff, A. Paracchino, K. Artuk, D. Jacobs, Q. Guesnay, F. Sahli, G. Andreatta, M. Boccard, Q. Jeangros, C. Ballif, *Science* **2023**, 381, 59.
[39] a)J. S. Manser, M. I. Saidaminov, J. A. Christians, O. M. Bakr, P. V. Kamat, *Acc Chem Res* **2016**, 49, 330; b)Q. Wang, Q. Dong, T. Li, A. Gruverman, J. Huang, *Adv Mater* **2016**, 28, 6734.
[40] W. J. Yin, T. T. Shi, Y. F. Yan, *Appl Phys Lett* **2014**, 104, 063903.
[41] a)R. Long, J. Liu, O. V. Prezhdo, *J Am Chem Soc* **2016**, 138, 3884; b)B. Chen, P. N. Rudd, S. Yang, Y. Yuan, J. Huang, *Chem Soc Rev* **2019**, 48, 3842.
[42] W. L. Tan, C. R. McNeill, *Applied Physics Reviews* **2022**, 9, 021310.
[43] A. Tejada, S. Braunger, L. Korte, S. Albrecht, B. Rech, J. A. Guerra, *Journal of Applied Physics* **2018**, 123, 175302.
[44] M. Soldera, K. Taretto, *Phys Status Solidi A* **2018**, 215, 1700906.
[45] H. Fujiwara, in *Spectroscopic Ellipsometry for Photovoltaics: Volume 1: Fundamental Principles and Solar Cell Characterization*, (Eds: H. Fujiwara, R. W. Collins), Springer International Publishing, Cham 2018.
[46] A. Bondaz, L. Kitzinger, C. Defranoux, *ECS Transactions* **2008**, 16, 33.
[47] S. Schorr, C. Stephan, T. Törndahl, R. Mainz, in *Advanced Characterization Techniques for Thin Film Solar Cells*, 2011.
[48] R. F. Egerton, in *Physical Principles of Electron Microscopy: An Introduction to TEM, SEM, and AEM*, (Ed: R. F. Egerton), Springer International Publishing, Cham 2016.
[49] a)S. Y. Leblebici, L. Leppert, Y. Li, S. E. Reyes-Lillo, S. Wickenburg, E. Wong, J. Lee, M. Melli, D. Ziegler, D. K. Angell, D. F. Ogletree, P. D. Ashby, F. M. Toma, J. B. Neaton, I. D. Sharp, A. Weber-Bargioni, *Nature Energy* **2016**, 1, 16093; b)W. Melitz, J. Shen, A. C. Kummel, S. Lee, *Surf Sci Rep* **2011**, 66, 1.
[50] a)W. Li, M. U. Rothmann, Y. Zhu, W. Chen, C. Yang, Y. Yuan, Y. Y. Choo, X. Wen, Y.-B. Cheng, U. Bach, J. Etheridge, *Nature Energy* **2021**, 6, 624; b)M. U. Rothmann, W. Li, J. Etheridge, Y. B. Cheng, *Advanced Energy Materials* **2017**, 7, 1700912; c)M. U. Rothmann, W. Li, Y. Zhu, U. Bach, L. Spiccia, J. Etheridge, Y. B. Cheng, *Nat Commun* **2017**, 8, 14547; d)M. U. Rothmann, J. S. Kim, J. Borchert, K. B. Lohmann, C. M. O'Leary, A. A. Sheader, L. Clark, H. J. Snaith, M. B. Johnston, P. D. Nellist, L. M. Herz, *Science* **2020**, 370, eabb5940.
[51] M. U. Rothmann, W. Li, Y. Zhu, A. Liu, Z. Ku, U. Bach, J. Etheridge, Y. B. Cheng, *Adv Mater* **2018**, 30, e1800629.
[52] Z. Ni, C. Bao, Y. Liu, Q. Jiang, W. Q. Wu, S. Chen, X. Dai, B. Chen, B. Hartweg, Z. Yu, Z. Holman, J. Huang, *Science* **2020**, 367, 1352.
[53] D. Shi, V. Adinolfi, R. Comin, M. Yuan, E. Alarousu, A. Buin, Y. Chen, S. Hoogland, A. Rothenberger, K. Katsiev, Y. Losovyj, X. Zhang, P. A. Dowben, O. F. Mohammed, E. H. Sargent, O. M. Bakr, *Science* **2015**, 347, 519.
[54] F. Yuan, Z. X. Wu, H. Dong, J. Xi, K. Xi, G. Divitin, B. Jiao, X. Hou, S. F. Wang, Q. H. Gong, *J Phys Chem C* **2017**, 121, 15318.
[55] D. L. Cao, W. B. Li, X. Zhang, L. Wan, Z. G. Guo, X. B. Wang, D. Eder, S. M. Wang, *J Mater Chem A* **2022**, 10, 19278.
[56] J. J. Xue, R. Wang, Y. Yang, *Nat Rev Mater* **2020**, 5, 809.
[57] L. Chen, J. W. Yoo, M. Hu, S. U. Lee, S. I. Seok, *Angew Chem Int Ed Engl* **2022**, 61, e202212700.
[58] G. Qu, D. Khan, F. Yan, A. Atsay, H. Xiao, Q. Chen, H. Xu, I. Nar, Z.-X. Xu, *Journal of Energy Chemistry* **2022**, 67, 263.

[59] E. H. Jung, B. Chen, K. Bertens, M. Vafaie, S. Teale, A. Proppe, Y. Hou, T. Zhu, C. Zheng, E. H. Sargent, *Acs Energy Lett* **2020**, 5, 2796.
[60] K. Choi, J. Lee, H. I. Kim, C. W. Park, G. W. Kim, H. Choi, S. Park, S. A. Park, T. Park, *Energ Environ Sci* **2018**, 11, 3238.
[61] a)L. Zuo, Q. Chen, N. De Marco, Y. T. Hsieh, H. Chen, P. Sun, S. Y. Chang, H. Zhao, S. Dong, Y. Yang, *Nano Lett* **2017**, 17, 269; b)S. Ullah, M. F. U. Din, J. K. Kasi, A. K. Kasi, K. Vegso, M. Kotlar, M. Micusik, M. Jergel, V. Nadazdy, P. Siffalovic, E. Majkova, A. Fakharuddin, *Acs Appl Nano Mater* **2022**, 5, 7822.
[62] S. Sonmezoglu, S. Akin, *Nano Energy* **2020**, 76, 105127.
[63] N. Guan, C. Ran, Y. Wang, L. Chao, Z. Deng, G. Wu, H. Dong, Y. Bao, Z. Lin, L. Song, *ACS Appl Mater Interfaces* **2022**, 14, 34198.
[64] E. Jiang, Y. Ai, J. Yan, N. Li, L. Lin, Z. Wang, C. Shou, B. Yan, Y. Zeng, J. Sheng, J. Ye, *ACS Appl Mater Interfaces* **2019**, 11, 36727.
[65] Y. Meng, C. Liu, R. Cao, J. Zhang, L. Xie, M. Yang, L. Xie, Y. Wang, X. Yin, C. Liu, Z. Ge, *Advanced Functional Materials* **2023**, n/a, 2214788.
[66] a)H. Li, C. Zhang, C. Gong, D. Zhang, H. Zhang, Q. Zhuang, X. Yu, S. Gong, X. Chen, J. Yang, X. Li, R. Li, J. Li, J. Zhou, H. Yang, Q. Lin, J. Chu, M. Grätzel, J. Chen, Z. Zang, *Nature Energy* **2023**; b)Y. Miao, X. Wang, H. Zhang, T. Zhang, N. Wei, X. Liu, Y. Chen, J. Chen, Y. Zhao, *eScience* **2021**, 1, 91; c)J. Wang, Z. Zhang, J. Liang, Y. Zheng, X. Wu, C. Tian, Y. Huang, Z. Zhou, Y. Yang, A. Sun, Z. Chen, C.-C. Chen, *Small* **2022**, 18, 2203886.
[67] H. X. Wang, W. Zhang, B. Y. Wang, Z. Yan, C. Chen, Y. Hua, T. Wu, L. Q. Wang, H. Xu, M. Cheng, *Nano Energy* **2023**, 111, 108363.
[68] J. H. Kim, Y. R. Kim, J. Kim, C. M. Oh, I. W. Hwang, J. Kim, S. Zeiske, T. Ki, S. Kwon, H. Kim, A. Armin, H. Suh, K. Lee, *Adv Mater* **2022**, 34, e2205268.
[69] a)Q. Wang, C. C. Chueh, T. Zhao, J. Cheng, M. Eslamian, W. C. H. Choy, A. K. Jen, *ChemSusChem* **2017**, 10, 3794; b)J. Mangalam, T. Rath, S. Weber, B. Kunert, T. Dimopoulos, A. Fian, G. Trimmel, *J Mater Sci-Mater El* **2019**, 30, 9602; c)H. Chen, A. Maxwell, C. Li, S. Teale, B. Chen, T. Zhu, E. Ugur, G. Harrison, L. Grater, J. Wang, Z. Wang, L. Zeng, S. M. Park, L. Chen, P. Serles, R. A. Awni, B. Subedi, X. Zheng, C. Xiao, N. J. Podraza, T. Filleter, C. Liu, Y. Yang, J. M. Luther, S. De Wolf, M. G. Kanatzidis, Y. Yan, E. H. Sargent, *Nature* **2023**, 613, 676.
[70] L. Liu, A. Mei, T. Liu, P. Jiang, Y. Sheng, L. Zhang, H. Han, *J Am Chem Soc* **2015**, 137, 1790.
[71] H. L. Yip, S. K. Hau, N. S. Baek, H. Ma, A. K. Y. Jen, *Advanced Materials* **2008**, 20, 2376.
[72] L. Zuo, Z. Gu, T. Ye, W. Fu, G. Wu, H. Li, H. Chen, *Journal of the American Chemical Society* **2015**, 137, 2674.
[73] A. Al-Ashouri, E. Köhnen, B. Li, A. Magomedov, H. Hempel, P. Caprioglio, J. A. Márquez, A. B. Morales Vilches, E. Kasparavicius, J. A. Smith, N. Phung, D. Menzel, M. Grischek, L. Kegelmann, D. Skroblin, C. Gollwitzer, T. Malinauskas, M. Jošt, G. Matič, B. Rech, R. Schlatmann, M. Topič, L. Korte, A. Abate, B. Stannowski, D. Neher, M. Stolterfoht, T. Unold, V. Getautis, S. Albrecht, *Science* **2020**, 370, 1300.
[74] a)T. Bu, J. Li, F. Zheng, W. Chen, X. Wen, Z. Ku, Y. Peng, J. Zhong, Y. B. Cheng, F. Huang, *Nat Commun* **2018**, 9, 4609; b)M. Abdi-Jalebi, Z. Andaji-Garmaroudi, S. Cacovich, C. Stavrakas, B. Philippe, J. M. Richter, M. Alsari, E. P. Booker, E. M. Hutter, A. J. Pearson, S. Lilliu, T. J. Savenije, H. Rensmo, G. Divitini, C. Ducati, R. H. Friend, S. D. Stranks, *Nature* **2018**, 555, 497; c)W. Chen, Y. C. Zhou, G. C. Chen, Y. H. Wu, B. Tu, F. Z. Liu, L. Huang, A. M. C. Ng, A. B. Djurisic, Z. B. He, *Advanced Energy Materials* **2019**, 9, 1803872.
[75] P. Y. Wang, B. B. Chen, R. J. Li, S. L. Wang, N. Y. Ren, Y. C. Li, S. Mazumdar, B. A. Shi, Y. Zhao, X. D. Zhang, *Acs Energy Lett* **2021**, 6, 2121.

[76] S. Liu, Y. Guan, Y. Sheng, Y. Hu, Y. Rong, A. Mei, H. Han, *Advanced Energy Materials* **2020**, 10, 1902492.
[77] a)X. Li, D. Bi, C. Yi, J. D. Decoppet, J. Luo, S. M. Zakeeruddin, A. Hagfeldt, M. Gratzel, *Science* **2016**, 353, 58; b)H. Zhang, M. K. Nazeeruddin, W. C. H. Choy, *Adv Mater* **2019**, 31, e1805702; c)M. Kim, G. H. Kim, T. K. Lee, I. W. Choi, H. W. Choi, Y. Jo, Y. J. Yoon, J. W. Kim, J. Lee, D. Huh, H. Lee, S. K. Kwak, J. Y. Kim, D. S. Kim, *Joule* **2019**, 3, 2179; d)M. Li, R. Sun, J. Chang, J. Dong, Q. Tian, H. Wang, Z. Li, P. Yang, H. Shi, C. Yang, Z. Wu, R. Li, Y. Yang, A. Wang, S. Zhang, F. Wang, W. Huang, T. Qin, *Nat Commun* **2023**, 14, 573.
[78] a)S. K. Gautam, M. Kim, D. R. Miquita, J. E. Bouree, B. Geffroy, O. Plantevin, *Advanced Functional Materials* **2020**, 30, 2002622; b)W. Rehman, D. P. McMeekin, J. B. Patel, R. L. Milot, M. B. Johnston, H. J. Snaith, L. M. Herz, *Energ Environ Sci* **2017**, 10, 361.
[79] a)D. J. Kubicki, D. Prochowicz, A. Hofstetter, S. M. Zakeeruddin, M. Grätzel, L. Emsley, *Journal of the American Chemical Society* **2017**, 139, 14173; b)J. Cao, S. X. Tao, P. A. Bobbert, C.-P. Wong, N. Zhao, *Advanced Materials* **2018**, 30, 1707350; c)D.-Y. Son, S.-G. Kim, J.-Y. Seo, S.-H. Lee, H. Shin, D. Lee, N.-G. Park, *Journal of the American Chemical Society* **2018**, 140, 1358.
[80] Y. Zhao, I. Yavuz, M. Wang, M. H. Weber, M. Xu, J.-H. Lee, S. Tan, T. Huang, D. Meng, R. Wang, J. Xue, S.-J. Lee, S.-H. Bae, A. Zhang, S.-G. Choi, Y. Yin, J. Liu, T.-H. Han, Y. Shi, H. Ma, W. Yang, Q. Xing, Y. Zhou, P. Shi, S. Wang, E. Zhang, J. Bian, X. Pan, N.-G. Park, J.-W. Lee, Y. Yang, *Nature Materials* **2022**, 21, 1396.
[81] a)J. Jeong, M. Kim, J. Seo, H. Lu, P. Ahlawat, A. Mishra, Y. Yang, M. A. Hope, F. T. Eickemeyer, M. Kim, Y. J. Yoon, I. W. Choi, B. P. Darwich, S. J. Choi, Y. Jo, J. H. Lee, B. Walker, S. M. Zakeeruddin, L. Emsley, U. Rothlisberger, A. Hagfeldt, D. S. Kim, M. Gratzel, J. Y. Kim, *Nature* **2021**, 592, 381; b)H. Lu, Y. Liu, P. Ahlawat, A. Mishra, W. R. Tress, F. T. Eickemeyer, Y. Yang, F. Fu, Z. Wang, C. E. Avalos, B. I. Carlsen, A. Agarwalla, X. Zhang, X. Li, Y. Zhan, S. M. Zakeeruddin, L. Emsley, U. Rothlisberger, L. Zheng, A. Hagfeldt, M. Gratzel, *Science* **2020**, 370, eabb8985.
[82] a)Q. Chang, F. Wang, W. Xu, A. Wang, Y. Liu, J. Wang, Y. Yun, S. Gao, K. Xiao, L. Zhang, L. Wang, J. Wang, W. Huang, T. Qin, *Angew Chem Int Ed Engl* **2021**, 60, 25567; b)H. Min, M. Kim, S. U. Lee, H. Kim, G. Kim, K. Choi, J. H. Lee, S. I. Seok, *Science* **2019**, 366, 749; c)B.-w. Park, H. W. Kwon, Y. Lee, D. Y. Lee, M. G. Kim, G. Kim, K.-j. Kim, Y. K. Kim, J. Im, T. J. Shin, S. I. Seok, *Nature Energy* **2021**, 6, 419.
[83] a)F. X. Xie, C. C. Chen, Y. Z. Wu, X. Li, M. L. Cai, X. Liu, X. D. Yang, L. Y. Han, *Energ Environ Sci* **2017**, 10, 1942; b)F. Ye, J. Ma, C. Chen, H. Wang, Y. Xu, S. Zhang, T. Wang, C. Tao, G. Fang, *Adv Mater* **2021**, 33, e2007126.
[84] N. J. Jeon, J. H. Noh, W. S. Yang, Y. C. Kim, S. Ryu, J. Seo, S. I. Seok, *Nature* **2015**, 517, 476.
[85] a)M. Saliba, T. Matsui, K. Domanski, J. Y. Seo, A. Ummadisingu, S. M. Zakeeruddin, J. P. Correa-Baena, W. R. Tress, A. Abate, A. Hagfeldt, M. Gratzel, *Science* **2016**, 354, 206; b)W. S. Yang, B. W. Park, E. H. Jung, N. J. Jeon, Y. C. Kim, D. U. Lee, S. S. Shin, J. Seo, E. K. Kim, J. H. Noh, S. I. Seok, *Science* **2017**, 356, 1376; c)E. H. Jung, N. J. Jeon, E. Y. Park, C. S. Moon, T. J. Shin, T. Y. Yang, J. H. Noh, J. Seo, *Nature* **2019**, 567, 511.
[86] T. Bu, J. Li, H. Li, C. Tian, J. Su, G. Tong, L. K. Ono, C. Wang, Z. Lin, N. Chai, X. L. Zhang, J. Chang, J. Lu, J. Zhong, W. Huang, Y. Qi, Y. B. Cheng, F. Huang, *Science* **2021**, 372, 1327.
[87] S. Mahesh, J. M. Ball, R. D. J. Oliver, D. P. McMeekin, P. K. Nayak, M. B. Johnston, H. J. Snaith, *Energ Environ Sci* **2020**, 13, 258.
[88] a)N. J. Jeon, J. H. Noh, Y. C. Kim, W. S. Yang, S. Ryu, S. I. Seok, *Nat Mater* **2014**, 13, 897; b)M. Xiao, F. Huang, W. Huang, Y. Dkhissi, Y. Zhu, J. Etheridge, A. Gray-Weale, U. Bach, Y. B. Cheng, L. Spiccia, *Angew Chem Int Ed Engl* **2014**, 53, 9898.
[89] D. Bi, C. Yi, J. Luo, J.-D. Décoppet, F. Zhang, Shaik M. Zakeeruddin, X. Li, A. Hagfeldt, M. Grätzel, *Nature Energy* **2016**, 1, 16142.
[90] Q. Cao, Y. Li, H. Zhang, J. Yang, J. Han, T. Xu, S. Wang, Z. Wang, B. Gao, J. Zhao, X. Li, X. Ma, S. M.

Zakeeruddin, W. E. I. Sha, X. Li, M. Gratzel, *Sci Adv* **2021**, 7, eabg0633.
[91] C. Ji, C. Liang, H. Zhang, M. Sun, F. Sun, Q. Song, X. Zhang, D. Li, F. You, Z. He, *Organic Electronics* **2018**, 63, 276.
[92] a)S. Valero, T. Soria, N. Marinovea, J. L. Delgado, *Polym Chem-Uk* **2019**, 10, 5726; b)F. Li, J. Yuan, X. Ling, Y. Zhang, Y. Yang, S. H. Cheung, C. H. Y. Ho, X. Gao, W. Ma, *Advanced Functional Materials* **2018**, 28, 1706377; c)Q. Cao, J. B. Yang, T. Wang, Y. K. Li, X. Y. Pu, J. S. Zhao, Y. X. Zhang, H. Zhou, X. Q. Li, X. H. Li, *Energ Environ Sci* **2021**, 14, 5406.
[93] S. Ghosh, S. Mishra, T. Singh, *Adv Mater Interfaces* **2020**, 7, 2000950.
[94] Y. Yuan, Q. Wang, Y. Shao, H. Lu, T. Li, A. Gruverman, J. Huang, *Advanced Energy Materials* **2016**, 6, 1501803.
[95] N. Pellet, P. Gao, G. Gregori, T.-Y. Yang, M. K. Nazeeruddin, J. Maier, M. Grätzel, *Angewandte Chemie International Edition* **2014**, 53, 3151.
[96] Z. Li, M. J. Yang, J. S. Park, S. H. Wei, J. J. Berry, K. Zhu, *Chem Mater* **2016**, 28, 284.
[97] Z. Xiao, Q. Dong, C. Bi, Y. Shao, Y. Yuan, J. Huang, *Adv Mater* **2014**, 26, 6503.
[98] D. Luo, W. Yang, Z. Wang, A. Sadhanala, Q. Hu, R. Su, R. Shivanna, G. F. Trindade, J. F. Watts, Z. Xu, T. Liu, K. Chen, F. Ye, P. Wu, L. Zhao, J. Wu, Y. Tu, Y. Zhang, X. Yang, W. Zhang, R. H. Friend, Q. Gong, H. J. Snaith, R. Zhu, *Science* **2018**, 360, 1442.
[99] Z. X. Jin, B. B. Yu, M. Liao, D. Liu, J. W. Xiu, Z. Zhang, E. Lifshitz, J. Tang, H. S. Song, Z. B. He, *Journal of Energy Chemistry* **2021**, 54, 414.
[100] J. Liu, C. Gao, X. He, Q. Ye, L. Ouyang, D. Zhuang, C. Liao, J. Mei, W. Lau, *ACS Appl Mater Interfaces* **2015**, 7, 24008.
[101] S. Xiao, Y. Bai, X. Y. Meng, T. Zhang, H. N. Chen, X. L. Zheng, C. Hu, Y. Q. Qu, S. H. Yang, *Advanced Functional Materials* **2017**, 27, 1604944.
[102] B. R. Li, T. G. Jiu, C. Y. Kuang, S. S. Ma, Q. S. Chen, X. D. Li, J. F. Fang, *Organic Electronics* **2016**, 34, 97.
[103] H. Yu, X. D. Liu, Y. J. Xia, Q. Q. Dong, K. C. Zhang, Z. W. Wang, Y. Zhou, B. Song, Y. F. Li, *J Mater Chem A* **2016**, 4, 321.
[104] T. Liu, X. Dong, J. Li, H. Liu, S. Wang, X. Li, *Science China Materials* **2021**, 64, 267.
[105] E. Akman, S. Akin, *Adv Mater* **2021**, 33, e2006087.
[106] R. Wang, J. Xue, K. L. Wang, Z. K. Wang, Y. Luo, D. Fenning, G. Xu, S. Nuryyeva, T. Huang, Y. Zhao, J. L. Yang, J. Zhu, M. Wang, S. Tan, I. Yavuz, K. N. Houk, Y. Yang, *Science* **2019**, 366, 1509.
[107] N. Aeineh, E. M. Barea, A. Behjat, N. Sharifi, I. Mora-Sero, *ACS Appl Mater Interfaces* **2017**, 9, 13181.
[108] a)D. Yao, C. Zhang, S. Zhang, Y. Yang, A. Du, E. Waclawik, X. Yu, G. J. Wilson, H. Wang, *ACS Appl Mater Interfaces* **2019**, 11, 29753; b)D. Zhang, X. Wang, Z. Fan, X. Xia, F. Li, *ACS Appl Mater Interfaces* **2022**, 14, 51053.
[109] a)R. Lin, Y. Wang, Q. Lu, B. Tang, J. Li, H. Gao, Y. Gao, H. Li, C. Ding, J. Wen, P. Wu, C. Liu, S. Zhao, K. Xiao, Z. Liu, C. Ma, Y. Deng, L. Li, F. Fan, H. Tan, *Nature* **2023**; b)K. T. Cho, S. Paek, G. Grancini, C. Roldan-Carmona, P. Gao, Y. H. Lee, M. K. Nazeeruddin, *Energ Environ Sci* **2017**, 10, 621.
[110] W. Yang, B. Ding, Z. Lin, J. Sun, Y. Meng, Y. Ding, J. Sheng, Z. Yang, J. Ye, P. J. Dyson, M. K. Nazeeruddin, *Adv Mater* **2023**, n/a, e2302071.
[111]a)H. Tsai, W. Nie, J. C. Blancon, C. C. Stoumpos, R. Asadpour, B. Harutyunyan, A. J. Neukirch, R. Verduzco, J. J. Crochet, S. Tretiak, L. Pedesseau, J. Even, M. A. Alam, G. Gupta, J. Lou, P. M. Ajayan, M. J. Bedzyk, M. G. Kanatzidis, *Nature* **2016**, 536, 312; b)T. Liu, J. Guo, D. Lu, Z. Xu, Q. Fu, N. Zheng, Z. Xie, X. Wan, X. Zhang, Y. Liu, Y. Chen, *ACS Nano* **2021**, 15, 7811; c)G. D. Li, J. Song, J. H. Wu, Z. Y. Song, X. B. Wang, W. H. Sun, L.

Q. Fan, J. M. Lin, M. L. Huang, Z. Lan, P. Gao, *Acs Energy Lett* **2021**, 6, 3614; d)H. Zhang, X. G. Ren, X. W. Chen, J. Mao, J. Q. Cheng, Y. Zhao, Y. H. Liu, J. Milic, W. J. Yin, M. Gratzel, W. C. H. Choy, *Energ Environ Sci* **2018**, 11, 2253; e)D. Yao, X. Mao, X. Wang, Y. Yang, N. D. Pham, A. Du, P. Chen, L. Wang, G. J. Wilson, H. Wang, *ACS Appl Mater Interfaces* **2020**, 12, 6651.

[112] C. C. Stoumpos, D. H. Cao, D. J. Clark, J. Young, J. M. Rondinelli, J. I. Jang, J. T. Hupp, M. G. Kanatzidis, *Chem Mater* **2016**, 28, 2852.

[113] a)L. Mao, W. Ke, L. Pedesseau, Y. Wu, C. Katan, J. Even, M. R. Wasielewski, C. C. Stoumpos, M. G. Kanatzidis, *J Am Chem Soc* **2018**, 140, 3775; b)X. Zhang, T. H. Yang, X. D. Ren, L. Zhang, K. Zhao, S. Z. Liu, *Advanced Energy Materials* **2021**, 11, 2002733; c)P. Fu, Y. Liu, S. W. Yu, H. Yin, B. W. Yang, S. Ahmad, X. Guo, C. Li, *Nano Energy* **2021**, 88, 106249.

[114] S. Ahmad, P. Fu, S. Yu, Q. Yang, X. Liu, X. Wang, X. Wang, X. Guo, C. Li, *Joule* **2019**, 3, 794.

[115] X. Q. Jiang, J. F. Zhang, S. Ahmad, D. D. Tu, X. Liu, G. Q. Jia, X. Guo, C. Li, *Nano Energy* **2020**, 75, 104892.

[116] T. Niu, Y.-M. Xie, Q. Xue, S. Xun, Q. Yao, F. Zhen, W. Yan, H. Li, J.-L. Brédas, H.-L. Yip, Y. Cao, *Advanced Energy Materials* **2022**, 12, 2102973.

[117] W. Li, X. Gu, C. Shan, X. Lai, X. W. Sun, A. K. K. Kyaw, *Nano Energy* **2022**, 91, 106666.

[118] W. Luo, C. Wu, D. Wang, Y. Zhang, Z. Zhang, X. Qi, N. Zhu, X. Guo, B. Qu, L. Xiao, Z. Chen, *ACS Appl Mater Interfaces* **2019**, 11, 9149.

[119] M. A. Green, E. D. Dunlop, J. Hohl-Ebinger, M. Yoshita, N. Kopidakis, K. Bothe, D. Hinken, M. Rauer, X. J. Hao, *Prog Photovoltaics* **2022**, 30, 687.

Acknowledgements

This work is sponsored by Shanghai Pujiang Program (22PJ1401200), the National Natural Science Foundation of China (No. U22A20142, No. 52302229), the Hebei Province Key Research and Development Project (No. 20314305D), China Huaneng Group Co., Ltd Headquarters Science and Technology Project (HNKJ20-H88).

Competing interests statement

The authors declare no competing interests.